arXiv:1405.6621v1 [math.NA] 26 May 2014

Adaptive Time Stepping for Vesicle Suspensions

Bryan Quaife[a], George Biros[a]

[a]*Institute of Computational Engineering and Sciences, The University of Texas at Austin, Austin, TX, 78712.*

Abstract

We present an adaptive arbitrary-order accurate time-stepping numerical scheme for the flow of vesicles suspended in Stokesian fluids. Our scheme can be summarized as an approximate implicit spectral deferred correction (SDC) method. Applying a textbook fully implicit SDC scheme to vesicle flows is prohibitively expensive. For this reason we introduce several approximations. Our scheme is based on a semi-implicit linearized low-order time stepping method. (Our discretization is spectrally accurate in space.) We also use invariant properties of vesicle flows, constant area and boundary length in two dimensions, to reduce the computational cost of error estimation for adaptive time stepping. We present results in two dimensions for single-vesicle flows, constricted geometry flows, converging flows, and flows in a Couette apparatus. We experimentally demonstrate that the proposed scheme enables automatic selection of the step size and high-order accuracy.

Keywords: Vesicle suspensions, Adaptive time stepping, Spectral deferred correction, Error control, Boundary integral equations, Integro-differential-algebraic equations, Fluid-structure interaction, particulate flows, Stokesian flows, Moving boundary problems

1. Introduction

Vesicles are deformable capsules filled with a viscous fluid. Vesicle flows refer to flow of vesicles that are suspended in a Stokesian fluid. Vesicles are differentiated from other capsules in the balance of forces in their interface. In particular, their boundary is locally inextensible (in 3D is locally incompressible). Vesicle flows find many applications many biological applications such as the simulation of biomembranes [36] and red blood cells [15, 22, 27, 28, 30].

The dynamics of a vesicle is governed by bending, tension (enforces inextensibility), hydrodynamics forces from other vesicles in the suspension, and possibly hydrodynamic forces from flow confinement boundary walls. Vesicle suspensions are modeled using the Stokes equations, a jump in the stress across each vesicle to match the interfacial forces on the membrane the vesicle, and a no-slip boundary condition on the vesicles and the confinement walls.

A significant challenge in simulating vesicle flows is that their governing equations are stiff. One stiffness source is associated with the interfacial forces, bending forces, and inextensibility related tension forces (depends mainly on the curvature of the vesicle). Another stiffness source is the hydrodynamic interaction between vesicles (depends on the minimum distance between vesicles). A third stiffness source is the hydrodynamic interaction between vesicles and external boundary walls (depends on the minimum distance between the vesicles and the wall). Therefore, to resolve the dynamics of a vesicle, it may be necessary to take a small time step when the vesicle has regions of large curvature, or when a vesicle approaches a boundary wall, or approaches another vesicle. However, a large time step may be taken when a vesicle has a smooth boundary and is separated from all other vesicles and the boundary walls. These considerations

Email addresses: quaife@ices.utexas.edu (Bryan Quaife), gbiros@acm.org (George Biros)

necessitate that we use an adaptive time-stepping scheme mostly for robustness of the code and to remove the need to manually select a time step size.

Another challenge in simulating vesicle flows is that maintaining good accuracy for long horizons requires a great number of time steps when using a low-order time-stepping method. Higher-order methods in time can mitigate error accumulation over long simulation times. However, implicit higher-order methods are quite challenging to combine with adaptive schemes. The most common methods are implicit multistep schemes, but those are problematic especially for dynamics that involve moving interfaces.

In summary, the design goals for a time-stepping scheme for vesicle flows is to address stiffness with reasonable computational costs, allow for adaptivity, and enable high-order time marching (at least second-order). In the past (in other groups as well as our group), methodologies have addressed parts of the design goals above, but no method, to our knowledge, address all of them. In this paper, we propose a scheme that provides this capability.

Summary of the method and contributions. To address stiffness, we use our recent work in which wall-vesicle, vesicle-vesicle, and bending-tension self interactions are treated implicitly [31]. There we used backward difference formulas (BDFs) with fixed time step sizes. As we discussed, it is possible to extend BDF with adaptive time stepping, but, since BDFs require the solution from multiple previous time step sizes but higher order methods become quite difficult to use in practice [14]. We develop a new high-order method that uses spectral deferred correction to iteratively increase the order of a first-order time integrator. By introducing SDC, we are able to iteratively construct high-order solutions that only require one previous time step.

In addition, we propose a time-stepping error estimation specific to vesicle flows. The incompressibility and inextensibility conditions require that the vesicle preserves both its enclosed area and total length. Thus, errors in area enclosed by a vesicle and errors in its perimeter can be used estimate the local truncation error. In this way we avoid forming multiple expensive solutions to estimate the local truncation error.

Our contributions are summarized below.

- We propose an SDC formulation to construct high-order solutions of an integro-differential-algebraic equation that governs vesicle suspensions.
- We propose an adaptive time stepping method that uses conserved quantities to estimate the local truncation error, therefore not requiring multiple numerical solutions to form this estimate.
- We conduct numerical experiments for several different flows involving multiple vesicles and confined flows that demonstrate the behavior of our scheme.

Related work. There is a rich literature on numerical methods for Stokesian particulate flows. We only discuss some representative time-stepping methods for vesicle flows and we omit details on the spatial discretization. Most methods for vesicle flows are based on integral equation formulations [32, 33, 35, 38, 41–43, 45, 46], but other formulations based on stencil discretizations also exist [3, 12, 23, 24].

The time-stepping schemes used for vesicle flows can be grouped in three classes of methods. The first class is fully explicit methods with a penalty formulation for the inextensibility constraint. These are relatively easy to implement but inefficient due to bending stiffness. Another class of methods treats self-interactions using linear semi-implicit time stepping. This addresses one main source of stiffness but they are fragile. No adaptive or higher than second-order scheme have been reported for these schemes. Finally, a third class of methods treat all the vesicle interactions using linearization and semi-implicit stepping. We are aware of two papers in this direction. In [46] a first order backward Euler scheme is used (with no adaptivity). As we mentioned in our own work [31, 34], we used a BDF scheme for vesicle flows that treats all interactions implicitly, but again, it is not adaptive and is accurate only up to second-order.

Finally, we briefly review the literature on SDC methods. SDC was first introduced by Dutt et al. [13]. SDC has been applied to partial differential equations [21, 39], differential algebraic equations [7, 20], and integro-differential equations [19], but not vesicle flows. In [26], Minion extended SDC to implicit-explicit

(IMEX) methods by studying the problem $\dot{\mathbf{x}}(t) = F_E(\mathbf{x}, t) + F_I(\mathbf{x}, t)$ where F_E is non-stiff and F_I is stiff. Unfortunately, our governing equations do not exhibit an additive splitting as non-stiff and stiff terms.

Algorithmically, SDC has been accelerated using preconditioners [18, 20] and parallel algorithms [8, 10, 11, 29, 39]. In our work, the SDC iterations are formed with first-order time methods. Higher-order methods can be used to form the iterations, and this is analyzed in [9]. However, such an analysis for integro-differential-algebraic equations is not the focus of this work.

Limitations. The main limitations of our approach are the following.

- We cannot provide a proof on the convergence order of our scheme. We will see in Section 5 that each SDC correction reduces the error significantly. However, when large numbers of SDC corrections are used, the asymptotic convergence rates are unclear. Minion observes similar behavior for stiff problems in [26]. Understanding the asymptotic rates of convergence could be used to further optimize the procedure for choosing optimal time step sizes.
- We have not explored the scheme for vesicle suspensions where the viscosity inside and outside each vesicles differs (viscosity contrast). The difficulty arises because flows with a viscosity contrast include a double-layer potential of the fluid velocity.
- Currently, each vesicle must use the same time step size. Therefore, in flows with multiple vesicles, the time step size is controlled by the vesicle requiring the smallest time step. This can result in the actual global error being much less than the desired error (see *Couette* example). Simulations could be accelerated if each vesicle could have its own time step size.

Let us remark that we do not use adaptivity in space.

Outline of the paper. In Section 2, we briefly discuss SDC for initial value problems (IVPs), and then discuss how to extend SDC to vesicle suspensions. In Section 3, we discretize the differential and integral equations arising in the SDC framework, discuss preconditioning, and provide complexity estimates. Section 4 discusses our adaptive time stepping strategy, and numerical results are presented in Section 5. Finally, we make concluding remarks in Section 6, and we reserve a more in depth formulation of our governing equations in the SDC framework Appendix A.

Notation. In Table 1, we summarize the main notation used in this paper.

2. Formulation

In this section, we briefly summarize the SDC formulation for IVPs and then extend SDC to an integro-differential equation that governs vesicle dynamics. We only discuss the theory of SDC and outline its numerical implementation in Section 3.

2.1. Spectral Deferred Correction

In its original development [13], SDC iteratively constructed a high-order solution of the IVP

$$\frac{d\mathbf{x}}{dt} = f(\mathbf{x}, t), \quad t \in [0, T], \quad \mathbf{x}(0) = \mathbf{x}_0. \tag{1}$$

While classical deferred correction methods discretize the time derivative in (1), SDC uses a Picard integral to avoid unstable numerical differentiation. Equation (1) is reformulated as

$$\mathbf{x}(t) = \mathbf{x}_0 + \int_0^t f(\mathbf{x}, \tau) d\tau, \quad t \in [0, T]. \tag{2}$$

Symbol	Definition
γ_k	Boundary of vesicle k
$\mathbf{x}_k(s,t)$	Parameterization of γ_k at time t and parameterized in arclength s
$\sigma_k(s,t)$	Tension of vesicle k at time t and parameterized in arclength s
Γ	Boundary of the confined geometry
$\mathcal{B}(\mathbf{x}_k)$	Bending operator due to vesicle k
$\mathcal{T}(\mathbf{x}_k)$	Tension operator due to vesicle k
$\mathrm{Div}(\mathbf{x}_k)$	Surface divergence operator due to vesicle k
$\mathcal{S}(\mathbf{x}_j,\mathbf{x}_k)$	Single-layer potential due to vesicle k and evaluated on vesicle j
$\mathcal{D}(\mathbf{x}_j,\Gamma)$	Double-layer potential due to Γ and evaluated on vesicle j
$\mathbf{v}_\infty(\mathbf{x}_j)$	Background velocity due to a far-field condition
$\mathbf{v}(\mathbf{x}_j;\mathbf{x}_k)$	Velocity of vesicle j due to hydrodynamic forces from vesicle k
$\mathbf{r}(t;\tilde{\mathbf{x}})$	Residual of equation (7) due to the provisional solution $\tilde{\mathbf{x}}$
$\mathbf{e}_{\mathbf{x}_j}$	Error between the exact vesicle position and the provisional position $\tilde{\mathbf{x}}_j$
e_{σ_j}	Error between the exact vesicle tension and the provisional tension $\tilde{\sigma}_j$
$A(t), L(t)$	Area and length of the vesicles at time t
e_A, e_L	Error in area and length
ϵ	Desired final tolerance for the area and length of the vesicles
$\beta_{\mathrm{up}} \geq 1$	Maximum amount the time step is allowed to be scaled up per time step
$\beta_{\mathrm{down}} \leq 1$	Minimum amount the time step is allowed to be scaled down per time step
$\alpha \leq 1$	Multiplicative safety factor for the new time step size

Table 1: *Index of frequently used notation.*

Any time stepping scheme can be used to generate a provisional solution $\tilde{\mathbf{x}}(t)$. Given this provisional solution $\tilde{\mathbf{x}}(t)$ of (2), the residual is defined as

$$\mathbf{r}(t;\tilde{\mathbf{x}}) = \mathbf{x}_0 - \tilde{\mathbf{x}}(t) + \int_0^t f(\tilde{\mathbf{x}},\tau)d\tau, \quad t \in [0,T]. \tag{3}$$

The integral in (3) is approximated by a p^{th}-order accurate quadrature rule. The error $\mathbf{e} = \mathbf{x} - \tilde{\mathbf{x}}$ satisfies

$$\mathbf{e}(t) = \mathbf{r}(t;\tilde{\mathbf{x}}) + \int_0^t (f(\tilde{\mathbf{x}}+\mathbf{e},\tau) - f(\tilde{\mathbf{x}},\tau))d\tau, \quad t \in [0,T], \tag{4}$$

and an approximation $\tilde{\mathbf{e}}$ of $\mathbf{e}$ is computed, generally using the same numerical method used to compute $\tilde{\mathbf{x}}$. Finally, the provisional solution is updated to $\tilde{\mathbf{x}} + \tilde{\mathbf{e}}$ and the procedure is repeated as many times as desired. The process of forming the residual $\mathbf{r}$, approximating the error $\mathbf{e}$, and updating the provisional solution is referred to as an SDC correction or iteration.

The accuracy of SDC depends on the discretization of (2) and (4) and the accuracy of the quadrature rule required to evaluate $\mathbf{r}(t;\tilde{\mathbf{x}})$. An abstract error analysis for applying deferred correction methods to the operator equation $F(y) = 0$ has been preformed in [4, 25, 37, 40]. In [17], this abstract framework was applied to (1) by defining $F(\mathbf{x}) = (-\mathbf{x}'(t) + f(\mathbf{x},t), -\mathbf{x}(0) + \mathbf{x}_0)$, and the main result is state in Theorem 4.2. Here we only summarize the result to avoid introducing additional notation.

Theorem 2.1. *Let $f \in C^\infty$ have bounded derivatives, and $\mathbf{x}$ be the unique solution of (1). Suppose that the time integrator ϕ is stable. That is, there exists some $S > 0$ which only depends on f and T, such that for all $\mathbf{y}, \mathbf{z} \in \mathbb{R}^m$,*

$$\|\mathbf{y} - \mathbf{z}\| \leq S\|\phi_m(\mathbf{y}) - \phi_m(\mathbf{z})\|.$$

Moreover, suppose that ϕ_m is of order k meaning that $\phi_m(\mathbf{x}) = \mathcal{O}(\Delta t^k)$, where $\Delta t = T/m$. Suppose that a numerical solution $\tilde{\mathbf{x}}$ of $\mathbf{x}$ satisfies

$$\|\tilde{\mathbf{x}}(T) - \mathbf{x}(T)\| \leq C\Delta t^\ell,$$

where C depends only on the derivatives of f and on T, but not on m. Assuming the residual $\mathbf{r}$ is computed exactly, if $\tilde{\mathbf{e}}$ is formed with the order p time integrator ϕ to approximate $\mathbf{e}$, then

$$\|\tilde{\mathbf{e}}(T) + \tilde{\mathbf{x}}(T) - \mathbf{x}(T)\| \leq C\Delta t^{\ell+k}.$$

However, since $\mathbf{r}$ is approximated with a p^{th}-order quadrature, the asymptotic error is

$$\|\tilde{\mathbf{e}}(T) + \tilde{\mathbf{x}}(T) - \mathbf{x}(T)\| = \mathcal{O}(\Delta t^{\min(\ell+k,p)}).$$

Theorem 2.1 tells us that by estimating the error $\mathbf{e}$ with a first-order method, which is the only order we consider in the SDC framework, the order of accuracy is increased by one, with the constraint that this convergence is limited by the accuracy of the quadrature rule for approximating (3). However, the theorem states nothing about the stability of SDC. In [13], the authors consider three discretizations of (2) and (4): fully explicit, fully implicit, and linear combinations of the two. We do not consider explicit methods since the governing equations are stiff. The other two methods could be used for vesicle suspensions, but both would require solving non-linear equations.

We have successfully used a variant of IMEX methods for vesicle suspensions [31, 33, 42], and we couple these methods with SDC in this work. IMEX methods [2] are a family of time integrators that treat some terms (generally, linear) implicitly and other terms explicitly. IMEX methods for additive splittings $\dot{\mathbf{x}}(t) = F_{\text{EXPLICIT}}(\mathbf{x},t) + F_{\text{IMPLICIT}}(\mathbf{x},t) = F_E(\mathbf{x},t) + F_I(\mathbf{x},t)$ of (1) were first applied to SDC by Minion in [26]. We summarize the numerical results from [26] since their behaviour resembles results that we will observe. First, the Van der Pol oscillator is considered in a non-stiff, mildly stiff, and stiff regime, and the number of SDC iterations ranges from two to six. In the non-stiff regime, the error behaves according to Theorem 2.1. In the mildly stiff case, the correct asymptotic result is observed, but not until Δt is much smaller. In the stiff regime, the convergence behaviour differs considerably from the formal error. This behaviour is attributed to order reduction which is further analyzed. The author proceeds to claim that "the correct asymptotic convergence rates would be observed given sufficiently small Δt; however, this is not the relevant issue in most applications". Two other examples considered are a system of differential equations resulting from a spatial discretization of an advection-diffusion equation, and Burgers equation. Convergence rates up to fifth-order are achieved. As before, as the system becomes stiffer, smaller time steps are required before the expected convergence behaviour is observed.

2.2. SDC for Vesicle Suspensions

Let $\{\gamma_j\}_{j=1}^M$ be a collection of vesicles parameterized by $\mathbf{x}_j$ and with tension σ_j (Figure 1). We use the integro-differential equation from [42] to balance the bending and tension forces of the vesicle with the stress jump of the fluid across the vesicle membrane, and an algebraic constraint to enforce the inextensibility condition. We start by defining the velocity of vesicle j due to the hydrodynamic forces from vesicle k

$$\mathbf{v}(\mathbf{x}_j;\mathbf{x}_k) = \mathbf{v}_\infty(\mathbf{x}_j)\delta_{j,k} + \mathcal{S}(\mathbf{x}_j,\mathbf{x}_k)(-\mathcal{B}(\mathbf{x}_k)(\mathbf{x}_k) + \mathcal{T}(\mathbf{x}_k)(\sigma_k)),$$

where $\delta_{j,k}$ is the Kronecker delta function,

$$\begin{aligned}
&s = \|\mathbf{x}'\|, \qquad \rho = \|\mathbf{x}-\mathbf{y}\|,\\
&\mathcal{S}(\mathbf{x}_j,\mathbf{x}_k)(\mathbf{f}) = \frac{1}{4\pi}\int_{\gamma_k}\left(-\log\rho + \frac{(\mathbf{x}-\mathbf{y})\otimes(\mathbf{x}-\mathbf{y})}{\rho^2}\right)\mathbf{f}(\mathbf{y})ds_{\mathbf{y}}, \quad \mathbf{x}\in\gamma_j,\\
&\mathcal{B}(\mathbf{x})(\mathbf{f}) = \frac{d^4\mathbf{f}}{ds^4},\\
&\mathcal{T}(\mathbf{x})(\sigma) = \frac{d}{ds}\left(\sigma\frac{d\mathbf{x}}{ds}\right),
\end{aligned}$$

and $\mathbf{v}_\infty$ is the background velocity (unconfined flows) or the velocity due to solid walls (confined flows). In the case of confined flows, we use the double-layer potential of an unknown density function $\boldsymbol{\eta}$ defined

on the boundary of the solid walls. The extra equation comes from a non-slip boundary condition on the solid walls and the details are presented in [33]. We point out that $\mathbf{v}$ is not symmetric, meaning that $\mathbf{v}(\mathbf{x}_j;\mathbf{x}_k) \neq \mathbf{v}(\mathbf{x}_k;\mathbf{x}_j)$ for all $j \neq k$, and $\mathcal{S}$, $\mathcal{B}$, $\mathcal{T}$ are all linear in their second argument.

The notation we are using is chosen so that terms such as $\mathcal{B}(\mathbf{x}^N)(\mathbf{x}^{N+1})$, which approximates $\mathcal{B}(\mathbf{x}^{N+1})(\mathbf{x}^{N+1})$, are understood to mean

$$\mathcal{B}(\mathbf{x}^N)(\mathbf{x}^{N+1}) = \frac{d^4}{ds^4}\mathbf{x}^{N+1}, \quad s = \|\mathbf{x}'^N\|,$$

where $\mathbf{x}'$ is the derivative of $\mathbf{x}$ with respect to its parameterization variable. The tension σ_j acts as a Lagrange multiplier to satisfy the inextensibility constraint

$$\mathrm{Div}(\mathbf{x}_j)\left(\sum_{k=1}^{M}\mathbf{v}(\mathbf{x}_j;\mathbf{x}_k)\right) = 0, \tag{5}$$

where

$$\mathrm{Div}(\mathbf{x})(\mathbf{f}) = \frac{d\mathbf{x}}{ds}\cdot\frac{d\mathbf{f}}{ds}, \quad s = \|\mathbf{x}'\|,$$

which is also linear in its second argument. Equation (5) can be eliminated using the Schur complement of the tension to write σ_j in terms of the positions $\mathbf{x}_k$, $k = 1,\ldots,M$. Then, $\mathbf{v}(\mathbf{x}_j;\mathbf{x}_k)$ can be written entirely in terms of $\mathbf{x}_j$ and $\mathbf{x}_k$, and the no-slip boundary condition of vesicle j gives

$$\frac{d\mathbf{x}_j}{dt} = \sum_{k=1}^{M}\mathbf{v}(\mathbf{x}_j;\mathbf{x}_k), \quad j = 1,\ldots,M. \tag{6}$$

The formulation (6) is easiest to present our numerical methods, but we in fact do not eliminate the tension in our implementation. The resulting changes to the SDC formulation are presented in Appendix A.

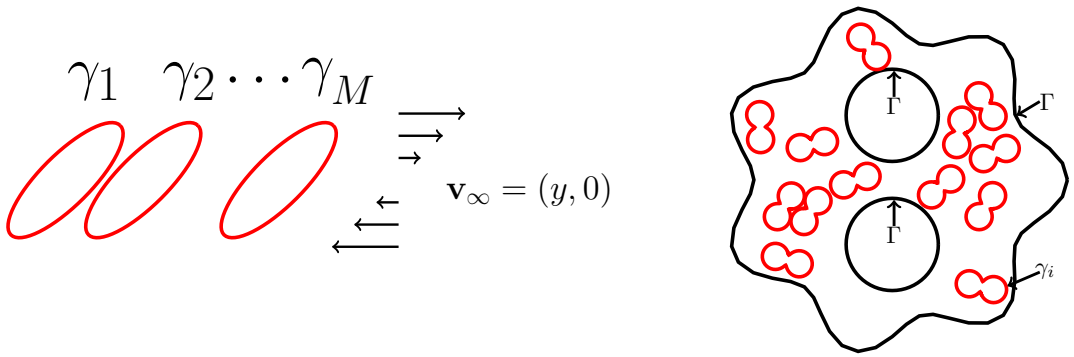

Figure 1: *Two typical vesicle suspensions. Left: M vesicles are submerged in an unbounded shear flow. Right:* 13 *vesicles are in a bounded domain. In the right configuration, the flow is driven by Dirichlet boundary conditions on Γ (The internal cylinders are rotating.)*

Following the SDC method we reformulate (6) as

$$\mathbf{x}_j(t) = \mathbf{x}_j(0) + \int_0^t \sum_{k=1}^{M}\mathbf{v}(\mathbf{x}_j;\mathbf{x}_k)d\tau, \quad t \in [0,T]. \tag{7}$$

We form a provisional solution $\tilde{\mathbf{x}}$ at a set of quadrature nodes in $[0, \Delta t]$ using a method that we describe in the next section (Section 3.4), and then evaluate

$$\mathbf{r}_j(t;\tilde{\mathbf{x}}) = \mathbf{x}_j(0) - \tilde{\mathbf{x}}_j(t) + \int_0^t \sum_{k=1}^{M} \mathbf{v}(\tilde{\mathbf{x}}_j;\tilde{\mathbf{x}}_k)d\tau, \quad t \in [0,T], \tag{8}$$

with a quadrature rule that we also define in the next section (Section 3.3). Then, the error $\mathbf{e}_{\mathbf{x}_j} = \mathbf{x}_j - \tilde{\mathbf{x}}_j$ satisfies

$$\mathbf{e}_{\mathbf{x}_j}(t) = \mathbf{x}_j(0) - \tilde{\mathbf{x}}_j(t) + \int_0^t \sum_{k=1}^{M} \mathbf{v}(\tilde{\mathbf{x}}_j + \mathbf{e}_{\mathbf{x}_j};\tilde{\mathbf{x}}_k + \mathbf{e}_{\mathbf{x}_k})d\tau, \quad t \in [0,T],$$

which we write using the residual $\mathbf{r}$ as

$$\mathbf{e}_{\mathbf{x}_j}(t) = \mathbf{r}_j(t;\tilde{\mathbf{x}}) + \int_0^t \sum_{k=1}^{M} (\mathbf{v}(\tilde{\mathbf{x}}_j + \mathbf{e}_{\mathbf{x}_j};\tilde{\mathbf{x}}_k + \mathbf{e}_{\mathbf{x}_k}) - \mathbf{v}(\tilde{\mathbf{x}}_j;\tilde{\mathbf{x}}_k))d\tau, \quad t \in [0,T]. \tag{9}$$

We define the new provisional solution as $\tilde{\mathbf{x}} + \tilde{\mathbf{e}}_{\mathbf{x}}$, where $\tilde{\mathbf{e}}_{\mathbf{x}}$ is an approximate solution of (9). Again, this procedure of computing the residual (8), numerically solving (9) for the error, and updating the provisional solution is what we call an SDC iteration. Assuming that we take n_{sdc} first-order SDC iterations and p is the quadrature error for computing the residual $\mathbf{r}$, from Theorem 2.1, we expect that the asymptotic rate of convergence is $\min(n_{\text{sdc}}, p)$.

3. Numerical Scheme

In this section, we present our numerical scheme for solving (7), (8), and (9). Evaluating $\mathbf{v}$ involves layer potentials and Fourier differentiation, and for concentrated suspensions, this can be costly. This cost will be further amplified in three-dimensional simulations (which are not discussed in this work). Therefore, we discretize (9) differently from standard methods of discretizing (4). We also discuss how the block-diagonal preconditioner outlined in [31] is applied. We conclude with estimates of the overall work per time step as a function of the number of vesicles and the number of points per vesicle.

3.1. Spatial Discretization

Following our previous work [31, 33, 42], we use a Lagrangian formulation by marking each vesicle with N tracker points. Since vesicles are modeled as smooth closed curves, all the derivatives are computed spectrally using the fast Fourier transform (FFT). Near-singular integrals are handled using the near-singular integration scheme outlined in [31]. Finally, we use Alpert's high-order Gauss-trapezoid quadrature rule [1] with accuracy $\mathcal{O}(h^8 \log h)$ to evaluate the single-layer potential, and the trapezoid rule for the double-layer potential which has spectral accuracy since its kernel is smooth.

3.2. Temporal Discretization

A fully explicit discretization of (6) results in a stiff system for multiple reasons. A stiffness analysis in [42] reveals that the leading sources of stiffness, and the corresponding time step restrictions, are:

- $\mathcal{S}(\mathbf{x}_j, \mathbf{x}_j)\mathcal{B}(\mathbf{x}_j)(\mathbf{x}_j)$ (self-hydrodynamic bending force) – $\Delta t \sim \Delta s^3$;
- $\mathcal{S}(\mathbf{x}_j, \mathbf{x}_j)\mathcal{T}(\mathbf{x}_j)(\mathbf{x}_j)$ (self-hydrodynamic tension force) – $\Delta t \sim \Delta s$;
- $\text{Div}(\mathbf{x}_j)(\mathbf{x}_j)$ (self-inextensibility force) – $\Delta t \sim \Delta s$;
- $\mathcal{S}(\mathbf{x}_j, \mathbf{x}_k)(\mathcal{B}(\mathbf{x}_k)(\mathbf{x}_k) + \mathcal{T}(\mathbf{x}_k)(\sigma_k))$, $j \neq k$ (inter-vesicle hydrodynamic forces) – depends on the inter-vesicle distance.

The leading sources of stiffness result from the intra-vesicle interactions; but, for concentrated suspensions, inter-vesicle interactions become significant and introduce stiffness.

To address these multiple sources of stiffness, we use a variant of IMEX [2] time integrators. IMEX methods were developed for the problem $\dot{\mathbf{x}}(t) = F_E(\mathbf{x}) + F_I(\mathbf{x})$, where F_E is non-stiff and is treated explicitly, and F_I is stiff and is treated implicitly. For problems with this additive splitting, the family of time integrators is

$$\frac{\beta \mathbf{x}^{n+1} - \mathbf{x}^0}{\Delta t} = F_E(\mathbf{x}^e) + F_I(\mathbf{x}^{n+1}),$$

where $\mathbf{x}^0$ and $\mathbf{x}^e$ are linear combinations of previous time steps and $\beta > 0$. Unfortunately, (6) does not have an additive splitting between stiff and non-stiff terms. However, we have observed first- and second-order convergence [31] for the time integrator

$$\frac{\beta \mathbf{x}_j^{n+1} - \mathbf{x}_j^0}{\Delta t} = \sum_{k=1}^{M} \mathbf{v}(\mathbf{x}_j^e; \mathbf{x}_k^{n+1}), \quad j = 1, \ldots, M,$$

where

$$\mathbf{v}(\mathbf{x}_j^e; \mathbf{x}_k^{n+1}) = \mathcal{S}(\mathbf{x}_j^e, \mathbf{x}_k^e)(-\mathcal{B}(\mathbf{x}_k^e)(\mathbf{x}_k^{n+1}) + \mathcal{T}(\mathbf{x}_k^e)(\sigma_k^{n+1})).$$

Note that in this formulation, it is the operators involved in $\mathbf{v}$, such as the bending $\mathcal{B}(\mathbf{x}_k)$ and the single-layer potential $\mathcal{S}(\mathbf{x}_j, \mathbf{x}_k)$, that are discretized explicitly at $\mathbf{x}^e$. In line with our previous work, we use the first-order method given by $\beta = 1$, $\mathbf{x}^0 = \mathbf{x}^n$, and $\mathbf{x}^e = \mathbf{x}^n$, and the second-order backward difference formula (BDF) given by $\beta = 3/2$, $\mathbf{x}^0 = 2\mathbf{x}^n - 1/2\mathbf{x}^{n-1}$, and $\mathbf{x}^e = 2\mathbf{x}^n - \mathbf{x}^{n-1}$.

3.3. Quadrature Formula

SDC requires a quadrature formula to approximate (8), the residual of the Picard integral. The quadrature rule effects the accuracy of SDC (Theorem 2.1). However, the stability of SDC is also effected by the quadrature rule, and this has been investigated in depth in [5]. We do not use equi-spaced nodes since they are vulnerable to the Runge phenomenon. In order to achieve the highest possible accuracy, we could use Gaussian nodes; however, in order to avoid extrapolation, we would like both endpoints to be quadrature nodes. Therefore, we use Gauss-Lobatto points, $0 = t_1 < \cdots < t_p = \Delta t$, since they include both endpoints, have maximal order $2p - 3$, and have successfully been used by other groups [5, 6, 26]. Alternatively, we could use Radau quadrature formula which include the left endpoint, but not the right.

For computational efficiency, the accuracy of the quadrature formula should not exceed the expected rate of convergence. This is especially important in three dimensions, which is not considered in this work, since multiple variables must be stored at each of the quadrature nodes for future SDC iterations.

3.4. Picard Integral Discretization

Equations (7) and (9) have similar structure, and we take advantage of this structure in their discretizations. For adaptivity, we want a scheme that easily allows for variable time step sizes. For this reason, we use only first-order methods for (7) and (9). When desired, we use SDC iterations to increase the accuracy.

The first-order provisional solution is found by discretizing (7) as

$$\mathbf{x}_j^{n+1} = \mathbf{x}_j^n + \Delta t_n \sum_{k=1}^{M} \mathbf{v}(\mathbf{x}_j^n; \mathbf{x}_k^{n+1}), \quad n = 0, \ldots, p-1, \tag{10}$$

where $\Delta t_n = t_{n+1} - t_n$. This is exactly the first-order time integrator we introduced in [31]. As we march in time with (10), we save the variables required for near-singular integration for future SDC iterations. Then, we evaluate the residual (8) using the Gauss-Lobatto quadrature rule.

In line with [26], which considers semi-implicit SDC methods, we would like to discretize (9) as

$$\mathbf{e}_{\mathbf{x}_j}^{n+1} = \mathbf{e}_{\mathbf{x}_j}^{n} + \mathbf{r}_j^{n+1} - \mathbf{r}_j^{n} + \Delta t_n \sum_{k=1}^{M} (\mathbf{v}(\tilde{\mathbf{x}}_j^n + \mathbf{e}_{\mathbf{x}_j}^n; \tilde{\mathbf{x}}_k^{n+1} + \mathbf{e}_{\mathbf{x}_k}^{n+1}) - \mathbf{v}(\tilde{\mathbf{x}}_j^n, \tilde{\mathbf{x}}_k^{n+1})).$$

The issue with this formulation is that it requires additional storage and computations to find the velocity due to the vesicle parameterized by $\tilde{\mathbf{x}}_k^n + \mathbf{e}_{\mathbf{x}_k}^n$. Again, in three dimensions this restriction is even more prohibitive. We have experimented with other discretizations of (9). The simplest such one is

$$\mathbf{e}_{\mathbf{x}_j}^{n+1} = \mathbf{e}_{\mathbf{x}_j}^{n} + \mathbf{r}_j^{n+1} - \mathbf{r}_j^{n}.$$

This discretization is consistent with the governing equations[1], but, experimentally, SDC converges only if a very small time step is used. To allow for larger time steps, we can include the implicit term in the discretization

$$\mathbf{e}_{\mathbf{x}_j}^{n+1} = \mathbf{e}_{\mathbf{x}_j}^{n} + \mathbf{r}_j^{n+1} - \mathbf{r}_j^{n} + \Delta t_n \sum_{k=1}^{M} (\mathbf{v}(\tilde{\mathbf{x}}_j^n; \tilde{\mathbf{x}}_k^{n+1} + \mathbf{e}_{\mathbf{x}_k}^{n+1}) - \mathbf{v}(\tilde{\mathbf{x}}_j^n; \tilde{\mathbf{x}}_k^{n+1})),$$

where we use a slight abuse of notation by defining

$$\mathbf{v}(\tilde{\mathbf{x}}_j^n; \tilde{\mathbf{x}}_k^{n+1} + \mathbf{e}_{\mathbf{x}_k}^{n+1}) = \mathcal{S}(\tilde{\mathbf{x}}_j^n, \tilde{\mathbf{x}}_k^n)(-\mathcal{B}(\tilde{\mathbf{x}}_k^n)(\tilde{\mathbf{x}}_k^{n+1} + \mathbf{e}_{\mathbf{x}_k}^{n+1}) + \mathcal{T}(\tilde{\mathbf{x}}_k^n)(\sigma_k^{n+1})).$$

(Note how none of the operators depend on the error $\mathbf{e}$.) Appendix refa:appendix1 presents this same discretization without the abuse of notation. While this discretization allows larger time steps, it is incompatible with the inextensibility constraint (see Appendix A). A discretization that is is compatible with the inextensibility constraint is

$$\mathbf{e}_{\mathbf{x}_j}^{n+1} = \mathbf{e}_{\mathbf{x}_j}^{n} + \mathbf{r}_j^{n+1} - \mathbf{r}_j^{n} + \Delta t_n \sum_{k=1}^{M} (\mathbf{v}(\tilde{\mathbf{x}}_j^{n+1}; \tilde{\mathbf{x}}_k^{n+1} + \mathbf{e}_{\mathbf{x}_k}^{n+1}) - \mathbf{v}(\tilde{\mathbf{x}}_j^{n+1}; \tilde{\mathbf{x}}_k^{n+1})), \tag{11}$$

where we are using the same abuse of notation. Note that (11) only requires evaluating the velocity field due to the vesicle configuration given by $\tilde{\mathbf{x}}_k^{n+1}$. Since these velocity fields are required to form residual $\mathbf{r}$, no additional velocity fields need to be formed. However, there is a loss in accuracy, but we have observed experimentally that if only one or two SDC corrections are used, it does not reduce the rate of convergence.

To summarize, the main steps for using SDC to solve (7) are

1. Find a first-order provisional solution $\tilde{\mathbf{x}}$ using (10).
2. Compute the residual $\mathbf{r}$ by approximating the integral in (8) with the Gauss-Lobatto quadrature rule.
3. Use (11) to approximate the error $\tilde{\mathbf{e}}$.
4. Define the new provisional solution to be $\tilde{\mathbf{x}} + \tilde{\mathbf{e}}$.
5. Go to step 2.

3.5. Preconditioning

Equations (10) and (11) are ill-conditioned and require a large number of GMRES iterations [42]. To reduce the cost of the linear solves, we used a block-diagonal preconditioner in [31] which is formed and factorized in matrix form at each time step. Using this preconditioner, the number of preconditioned GMRES iterations depends only on the magnitude of the inter-vesicle interactions, which in turn is a function

[1] If $\mathbf{e}_{\mathbf{x}_j}^n$ converges to 0, then $\mathbf{r}_j^{n+1} = \mathbf{r}_j^n$, and by (8), we have solved (7) up to quadrature error.

of the proximity of the vesicles. For further savings, we freeze and factorize the preconditioner at the first Gauss-Lobatto point, and this preconditioner is used for all the subsequent Gauss-Lobatto points and SDC iterates. By freezing the preconditioner, we significantly reduce the number of GMRES iterations, and we only require one matrix factorization per time step, which is the number of factorizations required when we precondition our time integrators introduced in [31].

3.6. Complexity Estimates

Here we summarize the cost of the most expensive algorithms required in our formulation.

- *Matrix-vector multiplication:* For unbounded flows, if M vesicles are each discretized with N points, the bending and tension calculations require $\mathcal{O}(MN \log N)$ operations using the FFT, and the single-layer potential requires $\mathcal{O}(MN)$ operations using the FMM. If the solid wall is discretized with N_{wall} points, using the FMM, the matrix-vector multiplication requires $\mathcal{O}(MN \log N + N_{\text{wall}})$ operations.
- *Computing the residual:* Given a provisional solution $\tilde{\mathbf{x}}$, computing the residual $\mathbf{r}$ is equivalent to p matrix-vector multiplications. Therefore, computing the residual requires $\mathcal{O}(p(MN \log N + N_{\text{wall}}))$ operations.
- *Forming the provisional solution and SDC corrections:* Equations (10) and (11) require solving the same linear system (only the right-hand sides are different), and our preconditioner results in a mesh-independent number of GMRES iterations. Therefore, if n_{gmres} total iterations are required to find the provisional solution, then n_{sdc} SDC iterations requires $\mathcal{O}(n_{\text{gmres}} p(n_{\text{sdc}} + 1)(MN \log N + N_{\text{wall}}))$ operations.
- *Forming the preconditioner:* The preconditioner is computed and stored in matrix form and requires $\mathcal{O}(MN^2 \log N)$ operations per time step by using Fourier differentiation and the FFT. The preconditioner must be factorized which requires $\mathcal{O}(MN^3)$ operations. This is computed only once per time step and is reused at all the additional Gauss-Lobatto quadrature points. In two-dimensions, this cost is acceptable since the number of unknowns on each vesicle is relatively small. However, in three-dimensions, this cost is unacceptable and different preconditioners will need to be constructed.

4. Adaptive Time Stepping

During the course of a simulation, vesicles come close to each other and to confining walls. For instance, as a vesicle passes through a constriction (see Figure 4), it can come very close to the solid wall and small time steps should be taken. Resolving multiple time scales is an important step towards a robust solver for vesicle suspensions for two reasons. First, the simulation is sped up since the largest possible time step is always taken, and second, we eliminate a trial and error procedure for finding a time step size that results in the desired tolerance.

A common strategy of an adaptive time step method is to control an estimate of the local truncation error. One estimate is the difference of two numerical solutions $\mathbf{x}_1$ and $\mathbf{x}_2$. One choice for $\mathbf{x}_1$ and $\mathbf{x}_2$ is the numerical solution formed from a single time step of size Δt and one formed from two time steps of size $\Delta t/2$ (step-doubling). Another choice is to use solutions formed by two different numerical methods whose orders differ by one. For vesicle suspensions, we can instead use two invariants to estimate the local truncation error. We use the errors in area and length, which are invariant by the incompressibility and inextensibility conditions, to estimate the local truncation error. This estimate does not require forming multiple numerical solutions.

We now outline how this estimate is used to accept or reject a time step, and how it is used to select a new time step size. Suppose we have a single vesicle[2] at time t with area $A(t)$, length $L(t)$, and the desired tolerance for the global error is ϵ at the time horizon $T = 1$. We compute the solution at time $t + \Delta t$ using a

[2] If there are multiple vesicles, we choose the minimum requested time step size over all of the vesicles.

k^{th}-order time stepping scheme which results in a new area $A(t+\Delta t)$ and length $L(t+\Delta t)$. First, we check if the solution at time $t+\Delta t$ satisfies

$$|A(t+\Delta t) - A(t)| \leq A(t)\Delta t\epsilon, \text{ and } |L(t+\Delta t) - L(t)| \leq L(t)\Delta t\epsilon. \tag{12}$$

If condition (12) is not satisfied, we reject this solution and we compute a new solution using a smaller time step size. If condition (12) is satisfied, we accept this solution and we increase the time step size so that we are taking the largest possible Δt such that (12) is satisfied for future time steps. As an alternative to fixing ϵ for the entire simulation, we experiment with increasing it as the simulation progresses in Section 5.4. The strategy is to increase ϵ at each time step to account for the fact that the actual error committed will be less than the predicted error. In this manner, the global error is much closer to the tolerance.

Regardless of the acceptance or rejection of the solution at time $t+\Delta t$, a new time step size must be chosen. We first require estimates of the asymptotic constants of proportionality for the errors in area and length

$$C_A = \frac{|A(t+\Delta t) - A(t)|}{A(t)\Delta t^{k+1}}, \text{ and } C_L = \frac{|L(t+\Delta t) - L(t)|}{L(t)\Delta t^{k+1}}.$$

We only consider the error in the area since the same argument can be applied to the error in length. The optimal time step size Δt_{opt} satisfies

$$|A(t+\Delta t_{\text{opt}}) - A(t)| = A(t)\Delta t_{\text{opt}}\epsilon, \tag{13}$$

and we also have the estimate

$$|A(t+\Delta t_{\text{opt}}) - A(t)| = C_A A(t)\Delta t_{\text{opt}}^{k+1}. \tag{14}$$

Equating (13) and (14), Δt_{opt} satisifies

$$C_A \Delta t_{\text{opt}}^{k+1} = \Delta t_{\text{opt}}\epsilon.$$

Finally, using our estimate for C_A, we have

$$\frac{|A(t+\Delta t) - A(t)|}{A(t)\Delta t^{k+1}}\Delta t_{\text{opt}}^{k+1} = \Delta t_{\text{opt}}\epsilon,$$

which implies that our next time step size should be

$$\Delta t_{\text{opt}} = \left(\frac{A(t)\epsilon\Delta t}{|A(t+\Delta t) - A(t)|}\right)^{1/k}\Delta t.$$

A similar optimal time step size is computed based on the length and the smaller of these two time steps is selected for the next time step.

We place restrictions on the new time step size to increase the probability of the next time step being accepted. Since our error estimates are local and asymptotic, it is dangerous to change the time step size too rapidly. Therefore, we restrict the new time step size scaling to the interval $[\beta_{\text{down}}, \beta_{\text{up}}]$, where $\beta_{\text{down}} < 1$ and $\beta_{\text{up}} > 1$. Next, we multiply the new time step size by a safety factor $\alpha^{1/k} < 1$ to increase the likelihood of the next time step size being accepted. Finally, we never increase the time step size if the previous time step size is rejected [16]. In summary, if the previous time step is accepted, the new time step size is

$$\Delta t_{\text{new}} = \alpha^{1/k}\min(\beta_{\text{up}}\Delta t, \max(\Delta t_{\text{opt}}, \beta_{\text{down}}\Delta t)),$$

and if the previous time step is rejected, the new time step size is

$$\Delta t_{\text{new}} = \alpha^{1/k}\min(\Delta t, \max(\Delta t_{\text{opt}}, \beta_{\text{down}}\Delta t)).$$

The scaling factor $\alpha^{1/k}$ is chosen so that

$$\max\left(\frac{|A(t+\Delta t)-A(t)|}{A(t)}, \frac{|L(t+\Delta t)-L(t)|}{L(t)}\right) \approx \alpha \Delta t \epsilon,$$

regardless of the order k. That is, with this scaling of α, the method tries to commit the same amount of error per time step, independent of the time stepping order.

The parameters α, β_{up}, and β_{down} affect the overall efficiency of the method. For instance, if α is too large, then Δt_{new} may be too large and the time steps will be rejected too often. However, if it is too small, the bounds in (12) will not be tight which will increase the total number of time steps. We have experimented with different values and have had success with $\alpha = \sqrt{0.9}$, $\beta_{\text{up}} = 1.5$ and $\beta_{\text{down}} = 0.6$. These values are used for all the numerical examples. We point out that when a small tolerance ϵ is chosen, the estimate (14) will be much more accurate, and β_{up} and β_{down} will not play a role since only small changes to the time step size will be made. However, when larger tolerances are requested, (14) is less accurate, and without β_{up} and β_{down}, unreasonable time step sizes may be chosen.

5. Results

We discuss the behaviour of SDC and adaptive time stepping for confined and unconfined flows. We are interested in problems whose dynamics exhibit multiple time scales, and problems with long time horizons. For such problems, it is beneficial that an adaptive time stepping takes the largest possible time steps and does not require a trial and error procedure to achieve a desired tolerance. The main parameters are:

- N: The number of points per vesicle;
- N_{wall}: The number of points per solid wall;
- m: The number of time steps used in the non-adaptive scheme;
- T: The time horizon;
- n_{sdc}: The number of SDC corrections;
- p: The number of Gauss-Lobatto quadrature points;
- β_{up}, β_{down}, α: Safety factors for adaptive time stepping as described in Section 4.

The simulations are performed in Matlab on a six-core 2.67GHz Intel Xeon processor with 24GB of memory. When appropriate, we also report the number of fast multiple method (FMM) calls which is the most expensive part of the simulations. We use four numerical examples of increasing complexity which we now summarize.

- **Relaxation** (Tables 2–4): We consider stiffness due to self-interactions by simulating a single vesicle in a Stokes fluid with no background velocity. Motivated by Theorem 2.1, we would like each additional SDC iteration to result in an additional order of accuracy.
- **Extensional** (Tables 5–9 and Figures 2–3): We consider stiffness due to vesicle-vesicle interactions by simulating two vesicles approaching each other in an extensional flow. We check the convergence of different time integrators and compare constant time step sizes and adaptive time step sizes.
- **Stenosis** (Tables 10–14 and Figures 4–6): We consider stiffness due to vesicle-wall interactions by simulating a single vesicle in a confined tube with a parabolic-profile flow at the intake and outtake. The vesicle passes through a narrow region where a smaller time step should be taken.
- **Couette** (Tables 15–17 and Figures 7–9): We consider eight vesicles in a Couette apparatus with a long time horizon. The solid walls are aligned so that there is a narrow region that the vesicles pass through. This examples involves all the stiff terms in our model.

Other details include:

- When using adaptive time stepping, no trial and error procedure to find a time step size that achieves the desired error is required. This is especially beneficial for simulations that require large amounts of CPU time due to long time horizons or concentrated suspensions.
- The area and length of the vesicles should be unchanged by the incompressibility and inextensibility constraints. Therefore, we use the error in area, e_A, and the error in length, e_L, to measure the error of the simulation, and to estimate the local truncation error required for adaptive time stepping.
- For the simulations we present, the interactions between the vesicles and solid walls are the most expensive part of the calculation. Therefore, for all examples except the first (it has no vesicle-vesicle or vesicle-boundary interactions), we report the total number of FMM calls (# fmm).
- For more concentrated suspensions, forming and factorizing the block-diagonal preconditioner is the most expensive part of the caculation. However, it is computed only once per time step in order to gurantee that the preconditioner is formed exactly once per time step for all the time integrators. When SDC is used, the preconditioner formed at the first Gauss-Lobatto point is used for all subsequent Gauss-Lobatto points and SDC corrections.
- For problems that use $n_{\text{sdc}} = 0$ or BDF, we do not use Gauss-Lobatto substeps. However, when $n_{\text{sdc}} > 0$, there are $m(p-1)$ time steps since the solution is required at the quadrature points to estimate $\mathbf{r}$.
- We take larger values of N than required in order to fully resolve the geometry, differential operators, and the layer potentials. This way, the temporal error, which is the main focus of this work, dominates the spatial error.
- All the linear systems are solved with GMRES without restarts (no GMRES solve requires more than 50 iterations) and with a tolerance of $1\text{E}{-10}$. We have experimented with tighter tolerances, but this has little or no effect on the reported errors and only increases the number of GMRES iterations. The reason that the errors do not decrease is that the condition number of the linear system, which for the report problems is on the order of $1\text{E}5$, restricts the minimum achievable residual.
- For the adaptive time stepping results, the time step size is never upscaled by more than $\beta_{\text{up}} = 1.5$, downscaled by more than $\beta_{\text{down}} = 0.6$, and the safety scaling factor is $\alpha = \sqrt{0.9}$. In addition, the time step size is never increased immediately after a rejected time step as is recommended in [16].

5.1. Relaxation

We consider a single vesicle, initialized as a three-to-one ellipse, in a Stokes fluid with no background velocity. We discretize the vesicle with $N = 96$ points and the time horizon is $T = 2$ which is large enough that the vesicle comes within 10% of its steady state solution. We use $p = 5$ Gauss-Lobatto quadrature points so that the quadrature's order of accuracy (seven in this case) is a few orders larger than the order of the time integrator (up to five). For this example, there are no calls to the FMM because the self-interactions are evaluated directly. We report the errors and CPU timings in Tables 2–4. We observe that:

- Each SDC iteration significantly improves the accuracy of the solution. However, we are unable to achieve third- and higher-order results. We expect that these convergence rates will be achieved for smaller values of Δt, but, at these required values for Δt, other sources of error, such as the GMRES tolerance or machine precision, will dominate. This behaviour is observed by Minion in [26].
- Comparing the left entires of Tables 2 and 3, we see that the CPU time increases by more than four-fold. This is a result of SDC having to form the solution at the intermediate Gauss-Lobatto points.
- Comparing the two second-order solvers (BDF and $n_{\text{sdc}} = 1$), we can not conclusively pick the faster method. However, simulations using SDC corrections are compatible with adaptive time stepping while with BDF, they are not.

	$\boldsymbol{n_{\mathbf{sdc}} = 0}$			**BDF**		
m	e_A	e_L	CPU	e_A	e_L	CPU
125	3.44E−6	3.40E−5	1.0	6.13E−8	1.56E−6	1.1
250	1.74E−6	1.74E−5	2.1	1.40E−8	3.57E−7	2.1
500	8.76E−7	8.83E−6	4.2	3.10E−9	7.84E−8	4.2
1000	4.40E−7	4.44E−6	8.4	2.41E−10	1.75E−8	8.3

Table 2: *The errors in area and length and the CPU time for a single vesicle in a* **relaxation** *flow with a* **constant** *time step size using* $\boldsymbol{n_{\mathbf{sdc}} = 0}$ *(left) and* **BDF** *(right). The CPU times for Tables 2–4 are relative to the cheapest simulation (*$m = 125$ *and* $n_{\text{sdc}} = 0$*) which took approximately 38 seconds. Both methods converge with their expected rate of convergence.*

	$\boldsymbol{n_{\mathbf{sdc}} = 1}$			$\boldsymbol{n_{\mathbf{sdc}} = 2}$		
m	e_A	e_L	CPU	e_A	e_L	CPU
125	2.75E−8	1.30E−8	4.6	3.99E−10	5.29E−11	7.2
250	7.28E−9	2.58E−9	9.0	1.98E−11	6.54E−12	16
500	1.88E−9	4.45E−10	17	1.04E−11	6.37E−13	29
1000	4.78E−10	6.88E−11	35	5.37E−12	4.77E−14	57

Table 3: *The errors in area and length and the CPU time for a single vesicle in a* **relaxation** *flow with a* **constant** *time step size using* $\boldsymbol{n_{\mathbf{sdc}} = 1}$ *(left) and* $\boldsymbol{n_{\mathbf{sdc}} = 2}$ *(right). We achieve second-order convergence with one SDC correction, but third-order convergence is only observed for the error in length with two SDC corrections. However, the error in area has plateaued which indicates that the GMRES tolerance has limited the error in area.*

	$\boldsymbol{n_{\mathbf{sdc}} = 3}$			$\boldsymbol{n_{\mathbf{sdc}} = 4}$		
m	e_A	e_L	CPU	e_A	e_L	CPU
125	9.77E−11	3.94E−13	10	1.10E−10	1.07E−14	13
250	2.03E−11	3.13E−14	20	2.74E−11	3.11E−15	26
500	4.30E−12	2.22E−15	41	6.60E−12	1.11E−16	49
1000	7.11E−13	1.33E−16	80	1.33E−12	1.44E−15	101

Table 4: *The errors in area and length and the CPU time for a single vesicle in a* **relaxation** *flow with a* **constant** *time step size using* $\boldsymbol{n_{\mathbf{sdc}} = 3}$ *(left) and* $\boldsymbol{n_{\mathbf{sdc}} = 4}$ *(right). The error in length achieves fourth-order convergence with three SDC corrections, but again, the error in area has plateaued. The error in area continues to plateau with four SDC corrections, and the error in length has reached machine precision.*

5.2. Extensional

We consider two vesicles placed symmetrically around the origin with the background velocity $\mathbf{v}_\infty = (-x, y)$ (Figure 2). We discretize both vesicles with $N = 96$ points and the time horizon is $T = 24$ which is long enough that the distance between the vesicles at the time horizon is $0.4\sqrt{\Delta s}$, where Δs is the arclength spacing. We use $p = 4$ Gauss-Lobatto quadrature points so that $\mathbf{r}$ has fifth-order accuracy which is at least two orders more accurate than all the reported time integrators. We report results using zero, one, and two SDC corrections, and BDF in Tables 5 and 6. Again, for some of the results, the expected convergence rates are not observed. Other groups (see, for example, [26, 44]) have observed that for stiff systems, very small time steps must be taken before the asymptotic convergence rates are achieved. As before, we expect that other sources of error will dominate once the temporal asymptotic regime is achieved.

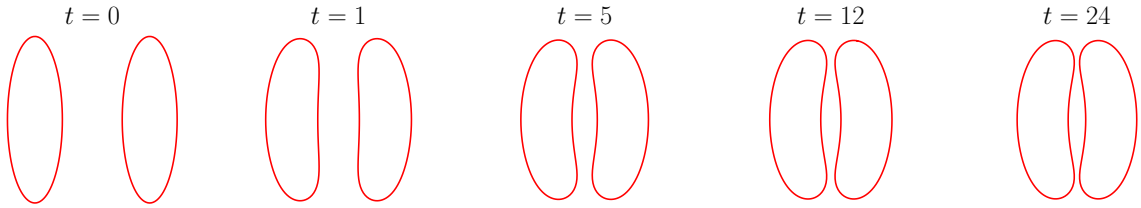

Figure 2: *Two vesicles discretized with $N = 96$ points. The vesicles are initially placed symmetrically around the origin and the background velocity is $\mathbf{v}_\infty = (-x, y)$.*

As the vesicles approach one another, their shape is nearly static and their velocities decrease. Therefore, we test our adaptive time stepping strategy using zero, one, and two SDC corrections. We expect that larger time steps can be taken as the vesicles come closer together. The errors in area and length, the number of accepted and rejected time steps, the number of FMM calls, and the CPU times are reported in Table 7 ($n_{\text{sdc}} = 0$), Table 8 ($n_{\text{sdc}} = 1$), and Table 9 ($n_{\text{sdc}} = 2$). The adaptive time stepping strategy does a good job of attaining the desired tolerance while not having too many rejected time steps. In Figure 3, we plot the time step size, the location of the rejected time steps, and the errors in area and length for a constant time step size and for an adaptive time step size. While the constant time step size commits a negligible amount of error shortly after the initial condition, too much error is accumulated at the beginning of the simulation. This indicates that a smaller time step should be taken near the start of the simulation, and then it can be increased later in the simulation. The left plot of Figure 3 exactly demonstrates this behaviour.

Comparing Tables 5–9, we observe the following behaviors:

- Unsurprisingly, the errors resulting from the first-order time integrator are much larger than those resulting from higher-order time integrators. These larger errors have a very adverse effect when using adaptive time stepping since very small time steps must be taken to maintain the requested local truncation error.
- As we saw in the *relaxation* example, the two second-order methods (BDF and $n_{\text{sdc}} = 1$) achieve similar errors with respect to CPU time. Again, only the integrator $n_{\text{sdc}} = 1$ is compatible with adaptive time stepping, so we no longer report results using BDF.
- Considering adaptive time steps, to achieve a four digits of accuracy, our second-order adaptive time integrator is 11 times faster than our first-order adaptive time integrator. Furthermore, if seven digits of accuracy is requested, our third-order adaptive time integrator is 23% faster.
- In general, when smaller tolerances are requested, additional SDC iterations, rather than smaller time step sizes, should be used to increase the accuracy. For instance, to achieve seven digits of accuracy, using two rather than one SDC correction results in a 25% savings in CPU time. This behaviour was also observed by Minion [26] for the Van der Pol equation: "higher-order methods are again more efficient when higher precision is required."

	$\boldsymbol{n_{\text{sdc}} = 0}$				**BDF**			
m	e_A	e_L	# fmm	CPU	e_A	e_L	# fmm	CPU
300	2.46E−4	1.27E−3	3.99E3	1.0	5.76E−5	5.67E−4	3.88E3	0.9
600	1.24E−4	6.64E−4	7.53E3	1.8	1.55E−5	2.00E−4	7.34E3	1.8
1200	6.24E−5	3.46E−4	1.44E4	3.6	4.12E−6	6.54E−5	1.40E4	3.6
2400	3.15E−5	1.79E−4	2.75E4	6.8	1.06E−6	1.92E−5	2.71E4	6.7

Table 5: *The errors in area and length and the CPU time for two vesicles in an* **extensional** *flow with a* **constant** *time step size using* $\boldsymbol{n_{\text{sdc}} = 0}$ *(left) and* **BDF** *(right). The CPU times for Tables 5–9 are relative to the cheapest simulation (*$m = 300$ *and* $n_{\text{sdc}} = 0$*) which took approximately 613 seconds. We achieve the desired first-order results, but second-order results are not yet achieved. With additional time steps, second-order convergence is achieved (see Table 7 in [31]).*

	$\boldsymbol{n_{\text{sdc}} = 1}$				$\boldsymbol{n_{\text{sdc}} = 2}$			
m	e_A	e_L	# fmm	CPU	e_A	e_L	# fmm	CPU
300	1.37E−6	3.08E−6	2.38E4	4.6	7.39E−7	7.16E−8	3.61E4	7.1
600	1.03E−6	1.32E−6	4.59E4	8.9	1.56E−7	8.78E−9	6.95E4	14
1200	4.51E−7	5.24E−7	8.91E4	18	3.26E−8	2.23E−9	1.35E5	26
2400	1.60E−7	1.76E−7	1.75E5	34	8.39E−9	7.25E−10	2.65E5	52
4800	4.95E−8	4.92E−8	3.46E5	67	2.90E−9	1.94E−10	5.28E5	104

Table 6: *The errors in area and length and the CPU time for two vesicles in an* **extensional** *flow with a* **constant** *time step size using* $\boldsymbol{n_{\text{sdc}} = 1}$ *(left) and* $\boldsymbol{n_{\text{sdc}} = 2}$ *(right). While each SDC correction reduces the error, the desired asymptotic rates of convergence are not achieved. As the ratios of successive errors are approaching the expected values, we expect that we have not taken enough time steps to observe the asymptotic rate of convergence. Also, we observe that one SDC correction and BDF have comparable errors with respect to computational work.*

Tolerance	e_A	e_L	Accepts	Rejects	# fmm	CPU
1E−2	2.10E−4	1.34E−3	76	28	1.16E3	0.3
1E−3	3.55E−5	2.22E−4	510	30	4.69E3	1.4
1E−4	6.73E−6	4.11E−5	4803	34	3.98E4	12

Table 7: *The errors in area and length, the CPU time, and the number of accepted and rejected time steps for two vesicles in an* **extensional** *flow with an* **adaptive** *time step size using* $\boldsymbol{n_{\text{sdc}} = 0}$*. For the larger tolerances, the desired tolerance is achieved in an acceptable amount of CPU time. However, first-order methods require too small of time steps to achieve four digits of accuracy. With these smaller tolerances, higher-order methods should be used.*

Tolerance	e_A	e_L	Accepts	Rejects	# fmm	CPU
1E−2	4.24E−3	2.93E−4	26	18	5.12E3	0.9
1E−3	2.90E−4	8.42E−5	28	16	4.32E3	0.8
1E−4	1.01E−6	7.10E−6	45	24	5.90E3	1.1
1E−5	7.08E−6	8.97E−7	97	16	8.14E3	1.5
1E−6	8.79E−7	4.40E−7	289	21	2.13E4	4.1
1E−7	9.18E−8	3.04E−9	891	24	6.07E4	12

Table 8: *The errors in area and length, the CPU time, and the number of accepted and rejected time steps for two vesicles in an* **extensional** *flow with an* **adaptive** *time step size and* $\boldsymbol{n_{\text{sdc}} = 1}$*. This second-order method is able to achieve much smaller tolerances than* $n_{\text{sdc}} = 0$*. However, when seven digits of accuracy is requested, the number of required time steps becomes unacceptable. In this case, a third-order method should be used.*

Tolerance	e_A	e_L	Accepts	Rejects	# fmm	CPU
1E−5	3.07E−6	1.53E−6	59	23	1.06E4	2.0
1E−6	6.48E−7	1.11E−7	143	33	2.06E4	4.0
1E−7	8.90E−8	1.68E−9	430	22	4.75E4	9.2

Table 9: *The errors in area and length, the CPU time, and the number of accepted and rejected time steps for two vesicles in an* **extensional** *flow with an* **adaptive** *time step size using* $\boldsymbol{n_{\text{sdc}} = 2}$*. We see that if smaller tolerances are desired, it is advantageous to use additional SDC corrections to allow for larger time steps.*

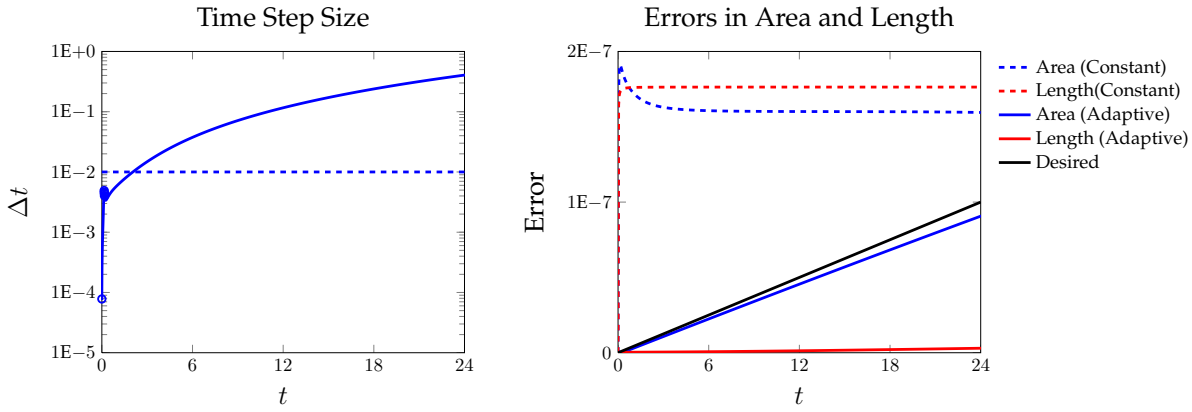

Figure 3: *Results for the* **extensional** *flow using* $\boldsymbol{n_{\text{sdc}} = 1}$. *Left: The time step size using 2400* **constant** *time step sizes (dashed) and an* **adaptive** *time step size (solid). The open circles indicate the 24 times when the time step size is rejected. As expected, the time step size increases as the vesicles come closer to a steady state. Right: The errors in area and length using* **constant** *(dashed) and* **adaptive** *(solid) time steps, and the desired error (black) of the adaptive time step. When using adaptive time stepping, the error in area nearly achieves the desired error indicating that we are almost selecting the optimal time step size. However, when using a constant time step size, a large amount of error is committed at the start of the simulation, and then very little error is committed for the duration of the simulation. The result is a nearly three-fold increase in the CPU time. The CPU time is further reduced by using adaptive time stepping with* $n_{\text{sdc}} = 2$.

5.3. Stenosis

We consider a single vesicle discretized with $N = 128$ points in a constricted tube discretized with $N_{\text{wall}} = 256$ points (Figure 4). At this resolution, our FMM implementation of the double-layer potential is slower than a direct evaluation. Therefore, the FMM is only used for the single-layer potentials. The time horizon is $T = 15$ which is sufficiently long that the vesicle passes through the constriction. We again use $p = 4$ Gauss-Lobatto quadrature points. We check the rates of convergence for a varying number of SDC corrections in Tables 10 and 11. We see that first- and second-order convergence is achieved in Table 10. While the error continues to decrease with each SDC iteration, as before, additional orders of convergence are not achieved for the presented values of Δt.

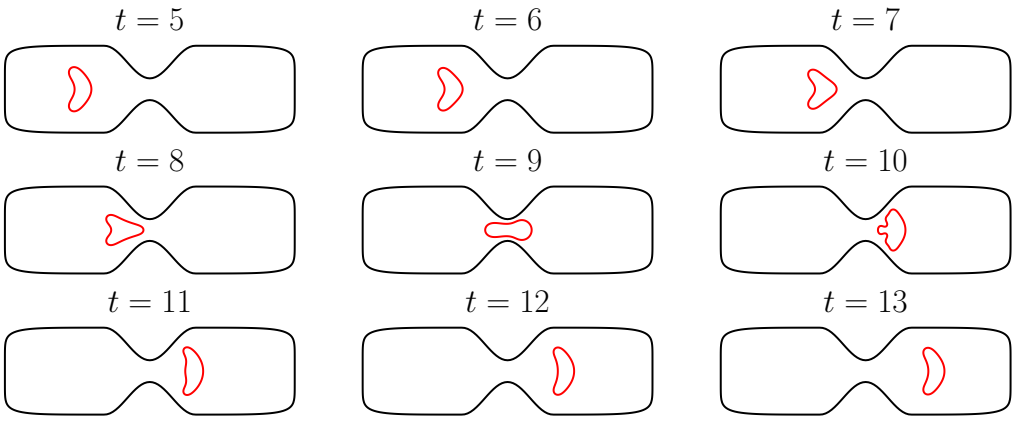

Figure 4: *A single vesicle discretized with* $N = 128$ *points passing through a constricted tube discretized with* $N_{\text{wall}} = 256$ *points. The boundary condition at the intake and outtake has a parabolic-profile and on the rest of the solid wall is zero.*

In Figure 5, we plot the errors in area and length using $n_{\text{sdc}} = 1$ and a constant time step size. Unsurprisingly, the errors increase when the vesicle passes through the constriction. In this interval, a smaller

time step should be taken. In Tables 12–14, we report results for adaptive time stepping with different tolerances and different numbers of SDC corrections. In Figure 6, we plot the errors in area and length using $n_{\text{sdc}} = 1$ with and without adaptive time stepping. We also plot the time step size and the location of the rejected time steps. As expected, a much smaller time step size is taken as the vesicle passes through the constriction.

We observe similar behavior as we observed for the *extensional* example. In particular,

- To achieve three digits of accuracy with $n_{\text{sdc}} = 0$, a fixed time step requires more than 6,000 time steps, and with adaptive time steps, over 30,000 time steps are required. This sharp increase is due to a very a small time step that must be taken to keep the local truncation error below the required threshold as the vesicle passes through the constriction (for this example, 65% of the time steps are smaller than 10^{-4}). Using the second-order integrator $n_{\text{sdc}} = 1$ with adaptive time stepping, only 172×3 adaptive time steps are required[3] are required to achieve 3 digits of accuracy. The resulting speedup is a factor of greater than 22.

- Comparing the two adaptive time stepping integrators $n_{\text{sdc}} = 1$ and $n_{\text{sdc}} = 2$, six digits of accuracy can be computed with 16% less CPU time by using $n_{\text{sdc}} = 2$. Again, this indicates that if smaller tolerances are desired, additional SDC corrections should be used to increase the accuracy of each time step.

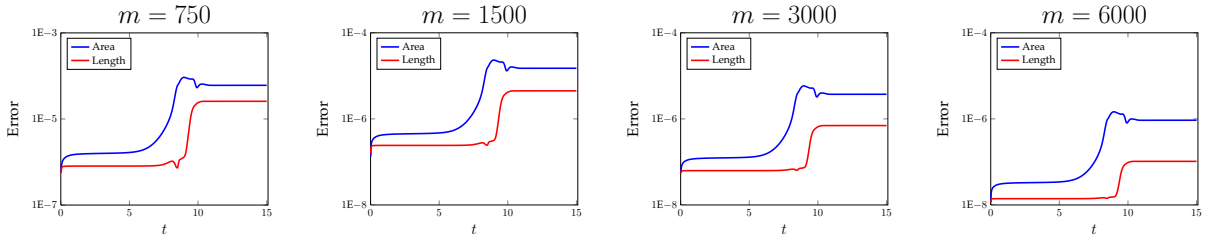

Figure 5: *The errors in area and length for a single vesicle in a constricted tube (***stenosis***) with a* **constant** *time step size using* $\boldsymbol{n_{\text{sdc}} = 1}$ *(right side of Table 10). Notice that the error increases sharply as the vesicle passes through the constriction for all the time step sizes. This indicates that a smaller time step size should be taken as the vesicle passes through the constriction.*

5.4. Couette

We consider eight vesicles discretized with $N = 192$ points in a couette apparatus where each wall is discretized with $N_{\text{wall}} = 512$ points (Figure 7). At this resolution, our FMM implementation of the double-layer potential is faster than a direct evaluation. Therefore, we use the FMM to evaluate all the single- and double-layer potentials. We use $p = 4$ Gauss-Lobatto quadrature points and take the long time horizon $T = 50$. At the time horizon, the inner boundary has made five complete rotations with a constant velocity, and the outer boundary is stationary. The inner and outer boundaries are aligned so that there is a narrow region that the vesicles must pass through. As a vesicle passes through this region, a smaller time step should be taken. We check the convergence rates with a constant time step size using zero and one SDC correction in Tables 15 and 16. For both time integrators, the expected first- and second-order convergence rates are achieved.

In Figure 8, we plot the errors in area and length using $n_{\text{sdc}} = 1$ with a constant time step size. If 500 time steps are taken, the error in length has a sharp jump caused by the blue vesicle in Figure 7. By reducing the time step size, the errors decrease at the expected rate, but there is still a jump in the errors near $t = 2$. In Table 17, we report results for $n_{\text{sdc}} = 1$ with adaptive time step sizes and two different tolerances. In

[3] Recall that $p - 1 = 3$ additional time steps are required because of the intermediate Gauss-Lobatto quadrature points.

	$\boldsymbol{n_{\mathbf{sdc}} = 0}$				$\boldsymbol{n_{\mathbf{sdc}} = 1}$			
m	e_A	e_L	# fmm	CPU	e_A	e_L	# fmm	CPU
750	1.16E−2	4.24E−2	1.90E4	1.0	6.05E−5	2.57E−5	1.26E5	6.9
1500	5.96E−3	2.12E−2	3.79E4	2.2	1.50E−5	4.48E−6	2.50E5	13
3000	3.03E−3	1.06E−2	7.55E4	4.2	3.73E−6	7.00E−7	4.96E5	26
6000	1.53E−3	5.28E−3	1.51E5	8.7	9.30E−7	1.03E−7	9.83E5	53

Table 10: *The errors in area and length and the CPU time for a single vesicle in a constricted tube (***stenosis***) with a* **constant** *time step size using $\boldsymbol{n_{\mathbf{sdc}} = 0}$ (left) and $\boldsymbol{n_{\mathbf{sdc}} = 1}$ (right). The CPU times for Tables 10–14 are relative to the cheapest simulation ($m = 750$ and $n_{\mathrm{sdc}} = 0$) which took approximately 2.30E3 seconds. We achieve the expected first- and second-order convergence rates.*

	$\boldsymbol{n_{\mathbf{sdc}} = 2}$				$\boldsymbol{n_{\mathbf{sdc}} = 3}$			
m	e_A	e_L	# fmm	CPU	e_A	e_L	# fmm	CPU
750	2.74E−5	1.08E−6	1.94E5	11	3.51E−7	4.38E−8	2.62E5	13
1500	7.16E−6	7.36E−8	3.84E5	21	5.97E−8	1.30E−9	5.19E5	27
3000	1.83E−6	5.31E−9	7.60E5	39	9.30E−9	4.60E−11	1.03E6	56
6000	4.63E−7	4.53E−10	1.51E6	81	1.35E−9	2.02E−12	2.03E6	108

Table 11: *The errors in area and length and the CPU time for a single vesicle in a constricted tube (***stenosis***) with a* **constant** *time step size using $\boldsymbol{n_{\mathbf{sdc}} = 2}$ (left) and $\boldsymbol{n_{\mathbf{sdc}} = 3}$ (right). We do not obtain the expected convergence rates, but we do see that each SDC correction does result in an increase in the accuracy. We could attempt to reach the asymptotic convergence rates, but this most likely would require temporal resolutions where other sources of error will dominate.*

Tolerance	e_A	e_L	Accepts	Rejects	# fmm	CPU
1E−2	2.57E−3	7.87E−3	3397	21	1.08E5	5.7
1E−3	2.95E−4	9.44E−4	33554	12	1.06E6	59

Table 12: *The errors in area and length, the CPU time, and the number of accepted and rejected time steps for a single vesicle in a constricted tube (***stenosis***) with an* **adaptive** *time step size using $\boldsymbol{n_{\mathbf{sdc}} = 0}$. Since the time integrator is first-order, small time steps have to be taken. The result is that the CPU time is too large at the reported tolerances.*

Tolerance	e_A	e_L	Accepts	Rejects	# fmm	CPU
1E−2	2.60E−3	8.03E−4	68	30	2.06E4	1.2
1E−3	5.55E−4	1.11E−4	172	68	4.80E4	2.6
1E−4	6.82E−5	1.18E−5	503	63	1.11E5	5.9
1E−5	7.20E−6	9.08E−7	1559	54	3.15E5	17
1E−6	7.35E−7	5.60E−8	4904	40	9.61E5	51

Table 13: *The errors in area and length, the CPU time, and the number of accepted and rejected time steps for a single vesicle in a constricted tube (***stenosis***) with an* **adaptive** *time step size using $\boldsymbol{n_{\mathbf{sdc}} = 1}$. This second-order method is able to take much larger time steps than the first-order method.*

Tolerance	e_A	e_L	Accepts	Rejects	# fmm	CPU
1E−5	7.19E−6	4.63E−8	828	136	2.96E5	16
1E−6	7.54E−7	2.49E−9	2558	105	8.21E5	43

Table 14: *The errors in area and length, the CPU time, and the number of accepted and rejected time steps for a single vesicle in a constricted tube (***stenosis***) with an* **adaptive** *time step size using $\boldsymbol{n_{\mathbf{sdc}} = 2}$. We see that if small tolerances are desired, additional SDC iterations should be used to achieve a higher-order time integrator.*

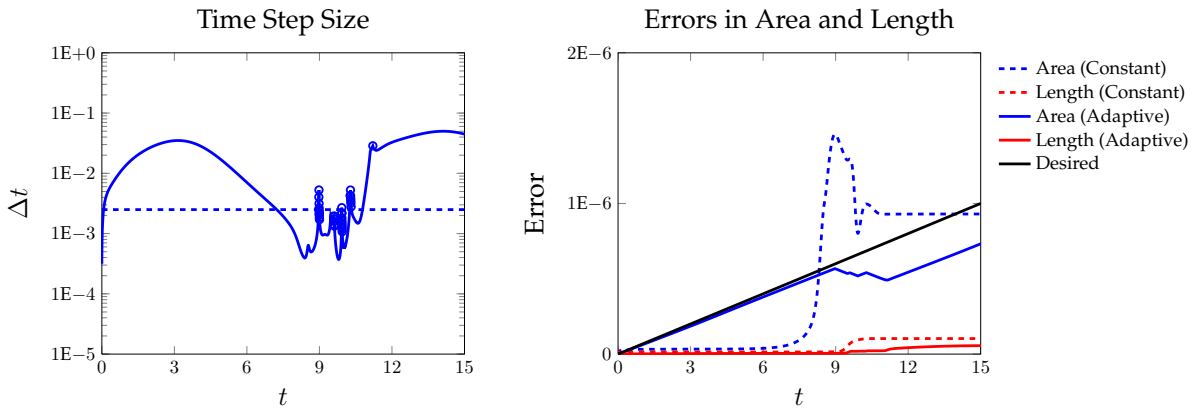

Figure 6: *Results for the* **stenosis** *flow using* $\boldsymbol{n_{\mathbf{sdc}} = 1}$. *Left: The time step size using 6000* **constant** *time step sizes (dashed) and an* **adaptive** *time step size (solid). The open circles indicate the 40 times when the time step size is rejected. Notice that the time step size decreases as the vesicle passes through the constriction. Right: The errors in area and length using* **constant** *(dashed) and* **adaptive** *(solid) time steps, and the desired error (black) of the adaptive time step. When using adaptive time stepping, the error in area nearly achieves the desired error everywhere except when the vesicle passes through the constriction, where the error in area actually drops. However, when using a constant time step size, very little error is committed at the start of the simulation, and then the majority of the error is committed as the vesicle passes through the constriction. Even though the CPU savings are negligible (it is about 4%), the adaptive time stepping method did not require any trial and error to find an appropriate time step size. The user simply specifies that they desire six digits accuracy and it is achieved. In addition, by using an additional SDC correction, the CPU savings is increased to 19%.*

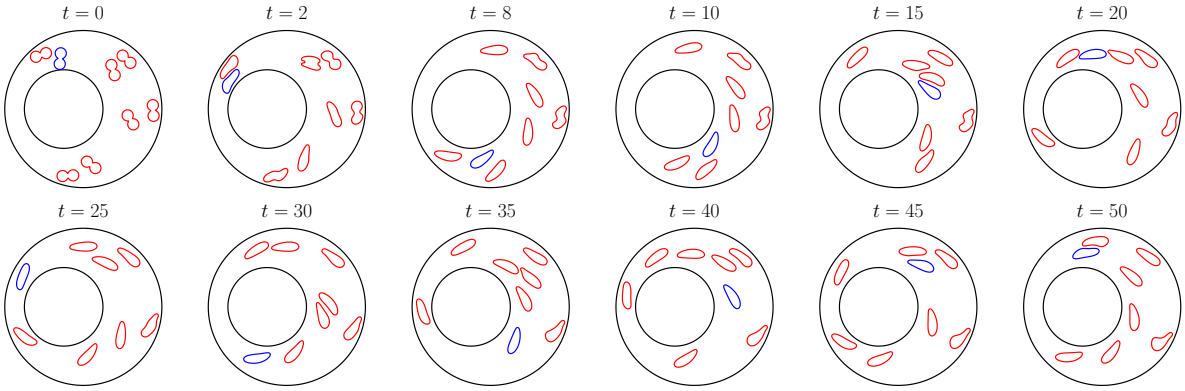

Figure 7: *Eight vesicles discretized with* $N = 192$ *points in a couette apparatus whose solid walls are each discretized with* $N_{\text{wall}} = 512$ *points. The outer boundary is stationary and the inner boundary has constant angular velocity and has completed five full rotations at* $T = 50$. *A single vesicle is colored in blue to help with visualization. The interactions between the vesicles and the solid walls complicate and simplify throughout the simulation and the simulation benefits from adaptive time stepping.*

Figure 9, we plot the errors in area and length with and without adaptive time stepping. We also plot the time step size and the locations of rejected time steps. We see that a small time step is taken initially as the vesicles smooth, and then much larger time steps can be taken once the vesicles are smooth and separated from one another and the solid walls.

While the desired error is achieved, the final error is much smaller than the tolerance when compared to the *extensional* and *stenosis* examples. This is a result of having more vesicles since the local truncation error is estimated with the maximum change in error, where the maximum is taken over all the vesicles. In contrast to the previous two examples, different vesicles commit the largest error at different times. The result is that the global error of our adaptive time stepping method is much less than the desired tolerance. A possible solution to this problem is to adjust the allowable truncation error at each time step. In particular, if we again assume that the time horizon is $T = 1$ and the desired tolerance is ϵ, then condition (12) is replaced with

$$|A(t + \Delta t) - A(t)| \leq A(t)\frac{\Delta t}{1 - t}\left(\epsilon - \frac{|A(t) - A(0)|}{A(0)}\right),$$

and a similar condition for the length. Using this new strategy with the time integrator from Table 17, with a tolerance of $1\text{E}{-1}$, the final error is $5.14\text{E}{-2}$, the number of accepted time steps is reduced to 222, but 84 time steps are rejected. Using a tolerance of $1\text{E}{-2}$, the final error is $9.62\text{E}{-3}$ with 583 accepted time steps, and the number of rejected time steps is only slightly increased to 74. While this strategy does offer a speedup, we expect that multiscale time integrators, where each vesicle's time step size can differ from the others', will overall result in a more robust solver.

We have also run the same simulation with a coarser discretization. We leave all the parameters unchanged with the exception of $N = 92$ points per vesicle and $N_{\text{wall}} = 192$ points per solid wall. Using adaptive time stepping with one SDC correction, a tolerance of $1\text{E}{-1}$ and $5\text{E}{-2}$ are attainable. However, with a tolerance of $1\text{E}{-2}$, the error condition (12) can not be satisfied at the initial condition for all Δt. Therefore, the spatial error is too large for condition (12) to be satisfied. We also ran this resolution at a later time when the vesicle shapes are smoothed. There, the desired local truncation error is attainable and the simulation can successfully complete. This indicates that spatial adaptivity is required, and this is a current extension we are developing.

Our conclusions from this example are:

- Considering the time integrator $n_{\text{sdc}} = 1$, to achieve one digit of accuracy, adaptive time stepping is at least 33% faster. However, to achieve two digits accuracy, with our current limitations (fixed spatial resolution, and each vesicle having the same time step size), adaptive time stepping does not conclusively offer a speedup. However, unlike the simulations with fixed time step size, no trial and error procedure to choose a time step size that results in the desired global error is required.
- With multiple vesicles, it is harder to achieve the desired global error. By adjusting the allowable local truncation error throughout the simulation, the final error is much closer to the tolerance. However, each vesicle must still have the same time step size. We plan to develop integrators that use different time step sizes for each vesicle.
- Without spatial adaptivity, excessively large resolutions are required for the entirety of the simulation.

6. Conclusions

We have developed and tested adaptive time stepping methods for an integro-differential equation used to simulate vesicle suspensions. To select the time step size, we followed the standard strategy of estimating the local truncation error, and then adjusting the time step size so that the same amount of error is committed per time step. This strategy does not require users to use a trial and error procedure to find a time step size that achieves the desirable error. Because of the cost of forming multiple numerical solutions,

	$\boldsymbol{n_{\mathbf{sdc}} = 0}$			
m	e_A	e_L	# fmm	CPU
2000	1.24E−1	3.50E−1	2.73E5	1.0
4000	2.04E−2	1.21E−1	5.28E5	2.1
8000	5.99E−3	5.79E−2	1.05E6	3.8

Table 15: *The errors in area and length and the CPU time for eight vesicles in a* **couette** *apparatus with a* **constant** *time step size using* $\boldsymbol{n_{\mathbf{sdc}} = 0}$*. The CPU for Tables 15–17 are relative to the cheapest simulation (*$m = 2000$ *and* $n_{\mathrm{sdc}} = 0$*) which took approximately* 1.44E5 *seconds. We achieve the expected first-order convergence.*

	$\boldsymbol{n_{\mathbf{sdc}} = 1}$			
m	e_A	e_L	# fmm	CPU
500	7.14E−3	5.39E−2	4.27E5	1.5
1000	2.79E−3	4.68E−5	8.28E5	2.9
2000	7.04E−4	9.34E−6	1.69E6	6.0

Table 16: *The errors in area and length and the CPU time for eight vesicles in a* **couette** *apparatus with a* **constant** *time step size using* $\boldsymbol{n_{\mathbf{sdc}} = 1}$*. At the reported resolutions, we are just beginning to achieve second-order convergence.*

Tolerance	e_A	e_L	Accepts	Rejects	# fmm	CPU
1E−1	2.65E−2	2.07E−2	256	68	2.90E5	1.0
1E−2	4.21E−3	3.86E−4	780	65	6.97E5	2.5

Table 17: *The errors in area and length, the CPU time, and the number of accepted and rejected time steps for eight vesicles in a* **couette** *apparatus with an* **adaptive** *time step size using* $\boldsymbol{n_{\mathbf{sdc}} = 1}$*.*

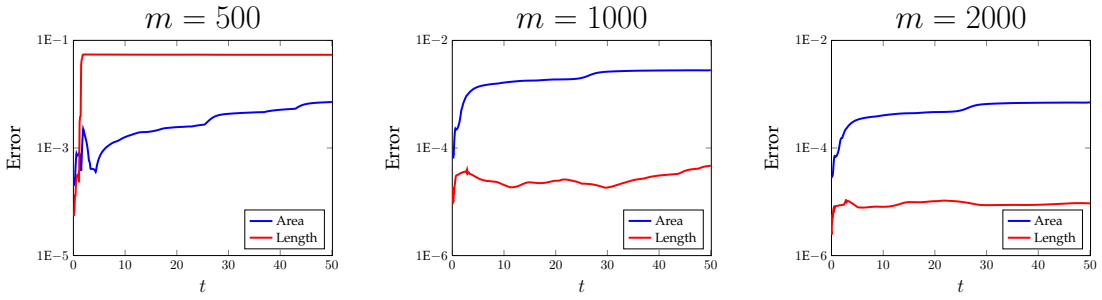

Figure 8: *The errors in area and length for eight vesicles in a* **couette** *apparatus with a* **constant** *time step size using* $\boldsymbol{n_{\mathbf{sdc}} = 1}$*. For all the time step sizes, there is a sharp increase in the errors around* $t = 2$ *which is committed by the vesicle colored in blue in Figure 7. Adaptive time stepping automatically resolves these sharp jumps and avoids the need to use trial and error to find an appropriate time step size.*

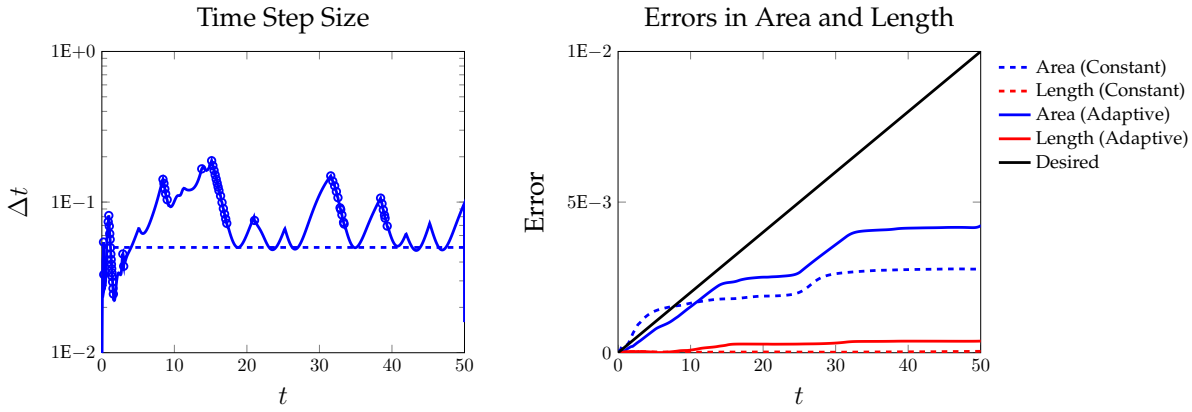

Figure 9: *Results for the* **couette** *apparatus using* $\boldsymbol{n_{\mathbf{sdc}} = 1}$. *Left: The time step size using a* **constant** *time step (dashed) and an* **adaptive** *time step size (solid). The open circles indicate the 65 times when the time step size is rejected. We see that the time step size is smallest when the error is large (near* $t = 2$*) and is largest when the vesicles and walls are well-separated (near* $t = 15$ *and* $t = 30$*). Right: The errors in area and length using* **constant** *(dashed) and* **adaptive** *(solid) time steps, and the desired error (black) of the adaptive time step. Since each vesicle must use the same time step size, the actual error does not closely follow the desired error.*

we introduced a technique where the error in area and length of the vesicles, which are fixed by the physics, are used to estimate the local truncation error. This method proved reliable, but it can only be applied to problems with measurable invariants.

In order to allow for larger time steps and longer time horizons, we introduced new high-order time integrators based on spectral deferred corrections (SDC). An advantage of these integrators is that they only require the solution from the previous time step making them compatible with adaptive time step sizes. To the best of our knowledge, this work is the first to apply IMEX methods coupled with SDC to a two-dimensional integro-differential equation. Therefore, we currently do not have any asymptotic results and our convergence results are entirely based on numerical results.

These contributions are a major step towards the development of a robust solver for vesicle suspensions, but several other features need to be introduced.

- Theoretical results, in particular the convergence rates of SDC, need to be developed. This will allow us to take the largest possible time step size given the user specified tolerance.
- Our SDC formulation does not support viscosity contrast. The challenge is that vesicle suspensions with viscosity contrast are governed by $\dot{\mathbf{x}} = F(\mathbf{x}, \dot{\mathbf{x}})$ which makes formulating a Picard integral difficult.
- Many suspensions would benefit from spatial adaptivity. This was demonstrated in the *couette* example where we saw that our adaptive time stepping method requires a sufficiently resolved spatial discretization, but this discretization was not required for the entirety of the simulation.
- All of our results are two-dimensional. However, none of the methods that we have introduced in this paper are restricted to two dimensions. Performing three-dimensional simulations only requires a careful implementation of the methods and the development of suitable preconditioners.

A. Complete SDC Formulation

Here we write our SDC formulation for the unbounded vesicle formulation that includes the tension σ_j. We also do not use the notation $\mathbf{v}(\mathbf{x}_j; \mathbf{x}_k)$ to help clarrify the discretization of the prediction and SDC

correction steps. Let $\tilde{\mathbf{x}}$ and $\tilde{\sigma}$ be a provisional solution of

$$\mathbf{x}_j(t) = \mathbf{x}_0 + \int_0^t \left(\mathbf{v}_\infty(\mathbf{x}_j) + \sum_{k=1}^{M} \mathcal{S}(\mathbf{x}_j, \mathbf{x}_k)(-\mathcal{B}(\mathbf{x}_k)(\mathbf{x}_k) + \mathcal{T}(\mathbf{x}_k)(\sigma_k)) \right) d\tau, \tag{15}$$

and then compute the residual

$$\mathbf{r}_j(t; \tilde{\mathbf{x}}, \tilde{\sigma}) = \mathbf{x}_0 - \tilde{\mathbf{x}}_j + \int_0^t \left(\mathbf{v}_\infty(\tilde{\mathbf{x}}_j) + \sum_{k=1}^{M} \mathcal{S}(\tilde{\mathbf{x}}_j, \tilde{\mathbf{x}}_k)(-\mathcal{B}(\tilde{\mathbf{x}}_k)(\tilde{\mathbf{x}}_k) + \mathcal{T}(\tilde{\mathbf{x}}_k)(\tilde{\sigma}_k)) \right) d\tau.$$

The error in the position is $\mathbf{e}_{\mathbf{x}_j} = \mathbf{x}_j - \tilde{\mathbf{x}}_j$, and the error in tension is $e_{\sigma_j} = \sigma_j - \tilde{\sigma}_j$. Substituting the errors into (15),

$$\begin{aligned}
\mathbf{e}_{\mathbf{x}_j}(t) = \mathbf{r}_j(t; \tilde{\mathbf{x}}, \tilde{\sigma}) &+ \int_0^t (\mathbf{v}_\infty(\tilde{\mathbf{x}}_j + \mathbf{e}_{\mathbf{x}_j}) - \mathbf{v}_\infty(\tilde{\mathbf{x}}_j)) d\tau \\
&- \int_0^t \sum_{k=1}^{M} \left(\mathcal{S}(\tilde{\mathbf{x}}_j + \mathbf{e}_{\mathbf{x}_j}, \tilde{\mathbf{x}}_k + \mathbf{e}_{\mathbf{x}_k}) \mathcal{B}(\tilde{\mathbf{x}}_k + \mathbf{e}_{\mathbf{x}_k}) - \mathcal{S}(\tilde{\mathbf{x}}_j, \tilde{\mathbf{x}}_k) \mathcal{B}(\tilde{\mathbf{x}}_k) \right) (\tilde{\mathbf{x}}_k) d\tau \\
&+ \int_0^t \sum_{k=1}^{M} \left(\mathcal{S}(\tilde{\mathbf{x}}_j + \mathbf{e}_{\mathbf{x}_j}, \tilde{\mathbf{x}}_k + \mathbf{e}_{\mathbf{x}_k}) \mathcal{T}(\tilde{\mathbf{x}}_k + \mathbf{e}_{\mathbf{x}_k}) - \mathcal{S}(\tilde{\mathbf{x}}_j, \tilde{\mathbf{x}}_k) \mathcal{T}(\tilde{\mathbf{x}}_k) \right) (\tilde{\sigma}_k) d\tau \\
&+ \int_0^t \sum_{k=1}^{M} \mathcal{S}(\tilde{\mathbf{x}}_j + \mathbf{e}_{\mathbf{x}_j}, \tilde{\mathbf{x}}_k + \mathbf{e}_{\mathbf{x}_k})(-\mathcal{B}(\tilde{\mathbf{x}}_k + \mathbf{e}_{\mathbf{x}_k})(\mathbf{e}_{\mathbf{x}_k}) + \mathcal{T}(\tilde{\mathbf{x}}_k + \mathbf{e}_{\mathbf{x}_k})(e_{\sigma_k})) d\tau.
\end{aligned} \tag{16}$$

For confined flows, $\mathbf{v}_\infty$ depends on yet another variable, a density function defined on the solid walls Γ, which we denote by $\boldsymbol{\eta}$. The dependence is through a double-layer potential $\mathcal{D}(\tilde{\mathbf{x}}_j, \Gamma)$. In this case, the term involving $\mathbf{v}_\infty$ in (16) becomes

$$\int_0^t (\mathcal{D}(\tilde{\mathbf{x}}_j + \mathbf{e}_{\mathbf{x}_j}, \Gamma) - \mathcal{D}(\tilde{\mathbf{x}}_j, \Gamma))(\boldsymbol{\eta}) d\tau,$$

and the final term in (16) includes the term $\mathcal{D}(\tilde{\mathbf{x}}_j + \mathbf{e}_{\mathbf{x}_j}, \Gamma)(\mathbf{e}_{\boldsymbol{\eta}_k})$.

The inextensibility constraint (5) is

$$\begin{aligned}
0 &= \mathrm{Div}(\mathbf{x}_j) \left(\mathbf{v}_\infty(\mathbf{x}_j) + \sum_{k=1}^{M} \mathcal{S}(\mathbf{x}_j, \mathbf{x}_k)(-\mathcal{B}(\mathbf{x}_k)(\mathbf{x}_k) + \mathcal{T}(\mathbf{x}_k)(\sigma_k)) \right) \\
&= \frac{d\mathbf{x}_j}{ds} \cdot \frac{d}{ds} \left(\mathbf{v}_\infty(\mathbf{x}_j) + \sum_{k=1}^{M} \mathcal{S}(\mathbf{x}_j, \mathbf{x}_k)(-\mathcal{B}(\mathbf{x}_k)(\mathbf{x}_k) + \mathcal{T}(\mathbf{x}_k)(\sigma_k)) \right),
\end{aligned} \tag{17}$$

and the errors satisfy

$$\begin{aligned}
0 =& \mathrm{Div}(\tilde{\mathbf{x}}_j + \mathbf{e}_{\mathbf{x}_j}) \left(\mathbf{v}_\infty(\mathbf{x}_j) \right. \\
&\left. + \sum_{k=1}^{M} \mathcal{S}(\tilde{\mathbf{x}}_j + \mathbf{e}_{\mathbf{x}_j}, \tilde{\mathbf{x}}_k + \mathbf{e}_{\mathbf{x}_k}) \left(-\mathcal{B}(\tilde{\mathbf{x}}_k + \mathbf{e}_{\mathbf{x}_k})(\tilde{\mathbf{x}}_k + \mathbf{e}_{\mathbf{x}_k}) + \mathcal{T}(\tilde{\mathbf{x}}_k + \mathbf{e}_{\mathbf{x}_k})(\tilde{\sigma}_k + e_{\sigma_k}) \right) \right).
\end{aligned} \tag{18}$$

A.1. Discretization

The provisional solution is found by discretizing (15) and (17) as

$$\mathbf{x}_j^{n+1} = \mathbf{x}_j^n + \Delta t_n \left(\mathbf{v}_\infty(\mathbf{x}_j^n) + \sum_{k=1}^{M} \mathcal{S}(\mathbf{x}_j^n, \mathbf{x}_k^n)(-\mathcal{B}(\mathbf{x}_k^n)(\mathbf{x}_k^{n+1}) + \mathcal{T}(\mathbf{x}_k^n)(\sigma_k^{n+1})) \right),$$

and

$$\mathrm{Div}(\mathbf{x}_j^n)\left(\sum_{k=1}^{M}\mathcal{S}(\mathbf{x}_j^n,\mathbf{x}_k^n)(-\mathcal{B}(\mathbf{x}_k^n)(\mathbf{x}_k^{n+1})+\mathcal{T}(\mathbf{x}_k^n)(\sigma_k^{n+1}))\right)=0.$$

The SDC updates (16) and (18) are discretized as

$$\mathbf{e}_{\mathbf{x}_j}^{n+1}=\mathbf{e}_{\mathbf{x}_j}^{n}+\mathbf{r}_j^{n+1}-\mathbf{r}_j^{n}+\Delta t_n\left(\sum_{k=1}^{M}\mathcal{S}(\tilde{\mathbf{x}}_j^{n+1},\tilde{\mathbf{x}}_k^{n+1})\left(-\mathcal{B}(\tilde{\mathbf{x}}_k^{n+1})(\mathbf{e}_{\mathbf{x}_k}^{n+1})+\mathcal{T}(\tilde{\mathbf{x}}_k^{n+1})(\delta_{\sigma_k}^{n+1})\right)\right),$$

and

$$\begin{aligned}&\mathrm{Div}(\tilde{\mathbf{x}}_j^{n+1})\left(\sum_{k=1}^{M}\mathcal{S}(\tilde{\mathbf{x}}_j^{n+1},\tilde{\mathbf{x}}_k^{n+1})\left(-\mathcal{B}(\tilde{\mathbf{x}}_k^{n+1})(\mathbf{e}_{\mathbf{x}_k}^{n+1})+\mathcal{T}(\tilde{\mathbf{x}}_k^{n+1})(\delta_{\sigma_k}^{n+1})\right)\right)\\&\qquad=-\mathrm{Div}(\tilde{\mathbf{x}}_j^{n+1})\left(\mathbf{v}_\infty(\tilde{\mathbf{x}}_j^{n+1})+\sum_{k=1}^{M}\mathcal{S}(\tilde{\mathbf{x}}_j^{n+1},\tilde{\mathbf{x}}_k^{n+1})\left(-\mathcal{B}(\tilde{\mathbf{x}}_k^{n+1})(\tilde{\mathbf{x}}_k^{n+1})+\mathcal{T}(\tilde{\mathbf{x}}_k^{n+1})(\tilde{\sigma}_k^{n+1})\right)\right).\end{aligned}$$

With this discretization of (18), we see that if $\mathbf{e}_{\mathbf{x}_k}^n=0$ and $\delta_{\sigma_k}^n=0$, then

$$\mathrm{Div}(\tilde{\mathbf{x}}_j^{n+1})\left(\mathbf{v}_\infty(\tilde{\mathbf{x}}_j^{n+1})+\sum_{k=1}^{M}\mathcal{S}(\tilde{\mathbf{x}}_j^{n+1},\tilde{\mathbf{x}}_k^{n+1})\left(-\mathcal{B}(\tilde{\mathbf{x}}_k^{n+1})(\tilde{\mathbf{x}}_k^{n+1})+\mathcal{T}(\tilde{\mathbf{x}}_k^{n+1})(\tilde{\sigma}_k^{n+1})\right)\right)=0,$$

which means that

$$\mathrm{Div}(\tilde{\mathbf{x}}_j^{n})\left(\sum_{k=1}^{M}\mathbf{v}(\tilde{\mathbf{x}}_j^{n};\tilde{\mathbf{x}}_k^{n})\right)=0.$$

In other words, by using the discretization (11), the fixed point of the SDC iteration exactly satisfies the inextensibility condition.

References

[1] B. K. Alpert. Hybrid Gauss-Trapezoidal Quadrature Rules. *SIAM Journal on Scientific Computing*, 20: 1551–1584, 1999.

[2] U.M. Ascher, S.J. Ruuth, and B.T.R. Wetton. Implicit-explicit methods for time-dependent partial differential equations. *SIAM Journal on Numerical Analysis*, 32:797–823, 1995.

[3] Thierry Biben, Klaus Kassner, and Chaouqi Misbah. Phase-field approach to three-dimensional vesicle dynamics. *Physical Review E*, 72(041921), 2005.

[4] K. Böhmer and H. J. Stetter. *Defect Correction Methods, Theory and Applications*. Springer-Verlag, New York, 1984.

[5] Anne Bourlioux, Anita T. Layton, and Michael L. Minion. High-Order Multi-Implicit Spectral Deferred Correction Methods for Problems of Reactive Flow. *Journal of Computational Physics*, 189:651–675, 2003.

[6] Elizabeth L. Bouzarth and Michael L. Minion. A multirate time integrator for regularized stokeslets. *Journal of Computational Physics*, 229(11):4208–4224, 2010.

[7] Sunyoung Bu, Jingfang Huang, and Michael L. Minion. Semi-implicit Krylov Deferred Correction Methods for Differential Algebraic Equations. *Mathematics of Computation*, 81:2127–2157, 2012.

[8] Andrew Christlieb and Benjamin Ong. Implicit Parallel Time Integrators. *Journal on Scientific Computing*, 49:167–179, 2010.

[9] Andrew Christlieb, Benjamin Ong, and Jing-Mei Qui. Comments on high order integrators embedded within integral deferred correction methods. *Communications in Applied Mathematics and Computational Science*, 4:27–56, 2009.

[10] Andrew J. Christlieb, Colin B. Macdonald, and Benjamin W. Ong. Parallel high-order integrators. *SIAM Journal on Scientific Computing*, 32(2):818–835, 2010.

[11] Andrew J. Christlieb, Ronald D. Haynes, and Benjamin W. Ong. A Parallel Space-Time Algorithm. *SIAM Journal on Scientific Computing*, 34(5):233–248, 2012.

[12] Qiang Du and Jian Zhang. Adaptive finite element method for a phase field bending elasticity model of vesicle membrane deformations. *SIAM Journal On Scientific Computing*, 30(3):1634–1657, 2007.

[13] A. Dutt, L. Greengard, and V. Rokhlin. Spectral Deferred Correction Methods for Ordinary Differential Equations. *BIT Numerical Mathematics*, 40:241–266, 2000.

[14] Werner Liniger Germund G. Dahlquist and Olavi Nevanlinna. Stability of Two-Step Methods for Variable Integration Steps. *SIAM Journal on Numerical Analysis*, 20(5):1071–1–85, October 1983.

[15] G. Ghigliotti, A. Rahimian, G. Biros, and C. Misbah. Vesicle Migration and Spatial Organization Driven by Flow Line Curvature. *Physical Review Letters*, 106:028101, 2011.

[16] Ernest Hairer, Gerhard Wanner, and Syvert Paul Nørsett. *Solving Ordinary Differential Equations I: Nonstiff Problems*. Springer, 1993.

[17] Anders C. Hansen and John Strain. On the order of deferred correction. *Applied Numerical Mathematics*, 61:961–973, 2011.

[18] Jingfang Huang, Jun Jia, and Michael Minion. Accelerating the convergence of spectral deferred correction methods. *Journal of Computational Physics*, 214:633–656, 2006.

[19] Jingfang Huang, Ming-Chih Lai, and Yang Xiang. An Integral Equation Method for Epitaxial Step-flow Growth Simulations. *Journal of Computational Physics*, 216:724–743, 2006.

[20] Jingfang Huang, Jun Jia, and Michael Minion. Arbitrary order Krylov deferred correction methods for differential algebraic equations. *Journal of Computational Physics*, 221(2):739–760, 2007.

[21] Jun Jia and Jingfang Huang. Krylov deferred correction accelerated method of lines transpose for parabolic equations. *Journal of Computational Physics*, 227:1739–1753, 2008.

[22] B. Kaoui, N. Tahiri, T. Biben, H. Ez-Zahraouy, A. Benyoussef, G. Biros, and C. Misbah. What Dictates Red Blood Cell Shapes and Dynamics in the Microvasculature? *Physical Review E*, pages 1–11, 2011.

[23] Yongsam Kim and Ming-Chih Lai. Simulating the dynamics of inextensible vesicles by the penalty immersed boundary method. *Journal of Computational Physics*, 229(12):4840–4853, 2010.

[24] Aymen Laadhari, Pierre Saramito, and Chaouqi Misbah. Computing the dynamics of biomembranes by combining conservative level set and adaptive finite element methods. *Journal of Computational Physics*, 263:328–352, 2014.

[25] Bengt Lindberg. Error estimation and iterative improvement for discretization algorithms. *BIT*, 20: 486–500, 1980.

[26] Michael L. Minion. Semi-Implicit Spectral Deferred Correction Methods for Ordinary Differential Equations. *Communications in Mathematical Sciences*, 1(3):471–500, 2003.

[27] C. Misbah. Vacillating Breathing and Tumbling of Vesicles under Shear Flow. *Physical Review Letters*, 96(2), 2006.

[28] H. Noguchi and D. G. Gompper. Shape transitions of fluid vesicles and red blood cells in capillary flows. *Proceedings Of The National Academy Of Sciences Of The United States Of America*, 102:14159–14164, 2005.

[29] Benjamin Ong, Andrew Melfi, and Andrew Christlieb. Parallel Semi-Implicit Time Integrators. *arxiv*, 2012. 1209.4297v1.

[30] C. Pozrikidis. The Axisymmetric Deformation Of A Red Blood Cell In Uniaxial Straining Stokes Flow. *Journal of Fluid Mechanics*, 216:231–254, 1990.

[31] Bryan Quaife and George Biros. High-volume fraction simulations of two-dimensional vesicle suspensions. *arxiv*, 2013. 1309.1128.

[32] Abtin Rahimian, Ilya Lashuk, Shravan K. Veerapaneni, Aparna Chandramowlishwaran, Dhairya Malhotra, Logan Moon, Rahul Sampath, Aashay Shringarpure, Jeffrey Vetter, Richard Vuduc, Denis Zorin, and George Biros. Petascale direct numerical simulation of blood flow on 200k cores and heterogeneous architectures. In *SC '10: Proceedings of the 2010 ACM/IEEE conference on Supercomputing*, pages 1–12, Piscataway, NJ, USA, 2010. IEEE Press.

[33] Abtin Rahimian, Shravan Kumar Veerapaneni, and George Biros. Dynamic simulation of locally inextensible vesicles suspended in an arbitrary two-dimensional domain, a boundary integral method. *Journal of Computational Physics*, 229:6466–6484, 2010.

[34] Abtin Rahimian, Shravan K. Veerapaneni, Denis Zorin, and George Biros. Fully discrete Galerkin Spectral Boundary Integral Method for Vesicle Flows with Viscosity Contrast. pages 1–28, 2012. Submitted for publication.

[35] C. Ramanujan, S. and Pozrikidis. Deformation of liquid capsules enclosed by elastic membranes in simple shear flow: large deformations and the effect of fluid viscosities. *Journal of Fluid Mechanics*, 361: 117–143, 1998.

[36] E. Sackmann. Supported membranes: Scientific and practical applications. *Science*, 271:43–48, 1996.

[37] Robert D. Skeel. A Theoretical Framework for Proving Accuracy Results for Deferred Corrections. *SIAM Journal on Numerical Analysis*, 19(1):171–196, 1982.

[38] J.S. Sohn, Y.-H. Tseng, S. Li, A. Voigt, and J.S. Lowengrub. Dynamics of multicomponent vesicles in a viscous fluid. *Journal of Computational Physics*, 229:119–144, January 2010.

[39] Robert Speck, Daniel Ruprecht, Matthew Emmett, Matthias Bolten, and Rolf Krause. A space-time parallel solver for the three-dimensional heat equation. In *Parallel Computing: Accelerating Computational Science and Engineering (CSE)*, volume 25 of *Advances in Parallel Computing*, pages 263 – 272. IOS Press, 2014.

[40] Hans J. Stetter. *Analysis of Discretization Methods for Ordinary Differential Equations*, volume 23. Springer Tracts in Natural Philosophy, 1973.

[41] S. Sukumaran and U. Seifert. Influence of shear flow on vesicles near a wall: A numerical study. *Physical Review Letter E*, 64(011916), 2001.

[42] S. K. Veerapaneni, D. Gueyffier, D. Zorin, and G. Biros. A boundary integral method for simulating the dynamics of inextensible vesicles suspended in a viscous fluid in 2D. *Journal of Computational Physics*, 228(7):2334–2353, 2009.

[43] Shravan K. Veerapaneni, Abtin Rahimian, George Biros, and Denis Zorin. A fast algorithm for simulating vesicle flows in three dimensions. *Journal or Computational Physics*, 230(14):5610–5634, 2011.

[44] Martin Weiser. Faster SDC convergence on non-equidistant grids by DIRK sweeps. Technical Report 13-30, ZIB, Takustr.7, 14195 Berlin, 2013.

[45] Hong Zhao and Eric S. G. Shaqfeh. The dynamics of a vesicle in simple shear flow. *Journal of Fluid Mechanics*, 674:578–604, 2011.

[46] Hong Zhao and Eric S. G. Shaqfeh. The dynamics of a non-dilute vesicle suspension in simple shear flow. *Journal of Fluid Mechanics*, 725:709–731, 2013.